



Article

A Framework for Optimizing Biomimetic Opaque Ventilated Façades Using CFD and Machine Learning

Ahmed Alyahya 1,* D, Simon Lannon 2 D and Wassim Jabi 2 D

- College of Architecture and Planning, Imam Abdulrahman Bin Faisal University, Dammam 31451, Saudi Arabia
- Welsh School of Architecture, Cardiff University, Cardiff CF10 3NB, UK; lannon@cardiff.ac.uk (S.L.); jabiw@cardiff.ac.uk (W.J.)
- * Correspondence: aaalyahya@iau.edu.sa

Abstract

This paper addresses the challenge of improving the thermal performance of building envelopes in hot arid climates by identifying optimal configurations for biomimetic opaque ventilated façade (OVF) designs. To overcome the complexity of parameter interactions in such systems, a multi-objective optimization framework is developed using computational fluid dynamics (CFD) simulations integrated with parametric modeling and machine learning surrogate models. A central contribution of this research is the application of machine learning-based surrogate models to predict CFD simulation outcomes with high accuracy. This predictive capability enables the rapid generation and evaluation of thousands of façade design alternatives without the need for full-scale CFD runs, significantly reducing computational effort and time. The proposed workflow establishes a direct connection between parameterized biomimetic geometries and thermal performance indicators, allowing for a comprehensive exploration of the design space through automated optimization. The optimization process relies on response surface modeling to approximate system behavior and evaluate design performance across multiple objectives. The final results reveal that the computationally optimized biomimetic façades achieved superior thermal performance compared to the initial bio-inspired design. To validate and extend the findings, additional simulations were carried out to evaluate the performance of selected designs under varying wind conditions and solar exposures. The larger wide mound configuration consistently performed best, offering a strong balance across the defined objectives. This solution was then applied to three-floor and five-floor commercial buildings in Riyadh, Saudi Arabia, where it showed a clear reduction in the average inner skin surface temperature of the OVF. The design proved suitable for construction with conventional methods and could be integrated into a range of architectural styles without major changes to the façade. These results reinforce the potential of combining biomimetic design strategies with computational optimization to develop high-performance façade systems for hot desert climates. The novelty of this work lies in combining biomimetic design principles with machine learningdriven optimization to systematically explore the design space and identify configurations that balance thermal efficiency with material economy.

Keywords: Opaque Ventilated Façades; Machine Learning; CFD; building envelope; computational design optimization; parametric design; biomimetic façade; Ansys DesignXplorer



Academic Editors: Xing Jin and Apple L.S. Chan

Received: 14 September 2025 Revised: 3 November 2025 Accepted: 13 November 2025 Published: 17 November 2025

Citation: Alyahya, A.; Lannon, S.; Jabi, W. A Framework for Optimizing Biomimetic Opaque Ventilated Façades Using CFD and Machine Learning. *Buildings* **2025**, *15*, 4130. https://doi.org/10.3390/ buildings15224130

Copyright: © 2025 by the authors. Licensee MDPI, Basel, Switzerland. This article is an open access article distributed under the terms and conditions of the Creative Commons Attribution (CC BY) license (https://creativecommons.org/licenses/by/4.0/).

Buildings **2025**, 15, 4130 2 of 32

1. Introduction

In performance-based architectural design, optimizing façade systems involves balancing multiple, often conflicting, objectives such as thermal performance, material efficiency, and constructability. Opaque ventilated façades (OVFs), particularly in hot arid climates, have demonstrated significant potential in reducing heat gain [1–4]. However, identifying optimal design configurations remains a complex task due to the intricate interplay of geometric and thermal parameters. While computational fluid dynamics (CFD) simulations provide detailed insights into the thermal behavior of such systems, their use as standalone tools is computationally intensive, especially when large numbers of design alternatives need to be evaluated.

To address this challenge, this study presents a computational framework that combines CFD simulations with parametric modeling and machine learning-based surrogate modeling to facilitate efficient multi-objective optimization of biomimetic OVF systems. Following an earlier concept and sensitivity analysis phase that identified a promising biomimetic geometry in the form of a wide mound design, as seen in Figure 1 [4], this phase focuses on optimizing its thermal performance using a multi-objective optimization workflow.

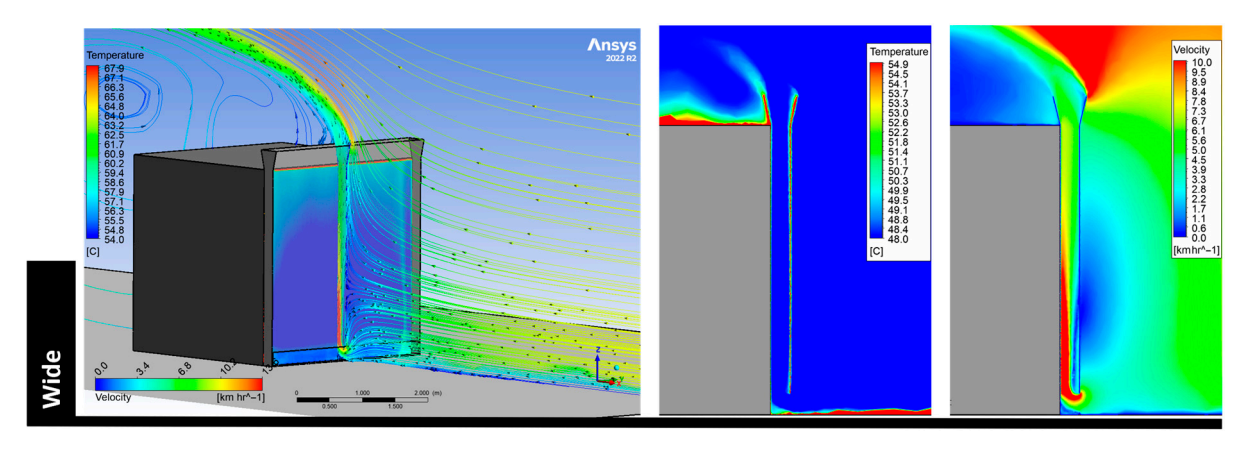


Figure 1. Wide mound biomimetic OVF design from the previous study [4].

Parametric modeling allows for the creation of digital models in which the geometric elements are defined by user-specified parameters. By modifying these parameters, a broad range of design options can be explored [5]. In this study, parametric modeling was used as a primary framework to represent the relationships between the given input parameters and the CFD outcomes. Among the available parametric modeling tools, the Grasshopper plugin for Rhinoceros [6] is the most widely adopted visual programming language in architectural research. The graphical algorithm editor in Grasshopper applies systematic logic to embed the design intent from the beginning and facilitates interaction with performance simulation tools and multi-objective evolutionary algorithm solvers for optimization.

However, since Ansys Fluent CFD software, 2022 [7] was selected for this study based on a comparison of widely accepted CFD tools in the preceding research on which this study is based [3], the parametric modeling had to be carried out within the Ansys Workbench platform. Ansys DesignXplorer [8] is a comprehensive system that uses a deterministic approach, incorporating Design of Experiments (DOE) and various optimization methods, with parameters playing a central role. These parameters can be defined within any compatible modeling tool, such as Ansys DesignModeler or Spaceclaim. The process involves solving the optimization problem using set objectives and parameters and identifying the best outcome by finding a suitable balance between those objectives [8]. As a result,

Buildings 2025, 15, 4130 3 of 32

the proposed biomimetic OVF solutions were redesigned and parameterized using the Spaceclaim block record feature to take full advantage of the DesignXplorer system.

Ansys DesignXplorer has been widely adopted in engineering disciplines for simulation-based optimization due to its ability to efficiently couple design of experiments (DOE), surrogate modeling, and sensitivity analysis with CFD tools. In recent research, the significance of Ansys DesignXplorer has been underscored for optimizing flow characteristics in curved conduits. This tool facilitates efficient parametric studies, significantly reducing the number of required CFD simulations [9]. By employing response surface methodology, DesignXplorer enables rapid exploration of various vane configurations, which significantly cuts down computational time [9]. Furthermore, its capability to manage multi-objective optimization allows users to effectively balance the trade-offs between minimizing pressure drop and maximizing velocity uniformity, guiding the design process toward optimal solutions [9]. The integration of DesignXplorer with Ansys Fluent ensures that the optimization results are grounded in reliable CFD simulations, enhancing the overall accuracy of the outcomes [9]. In another study, Ayancik et al. (2016) [10] highlight the necessity of using sophisticated optimization techniques to ensure the creation of cavitation-free runner blades with high efficiency. The study highlights the significance of balancing conflicting goals, such as enhancing efficiency and reducing the risk of cavitation [10]. By adopting this strategy, the design process becomes more efficient, and turbine performance is improved, underscoring the essential role of advanced optimization techniques in hydraulic engineering [10]. These examples highlight the versatility of DesignXplorer for high-fidelity CFD-based optimization, enabling significant performance improvements while reducing computational cost.

In building performance research, optimization methods have emerged as vital tools for enhancing architectural design variables. Kaseb and Montazeri (2022) [11] investigated the aerodynamic optimization of building-integrated ducted openings using metamodeling techniques. Their study revealed that such optimization significantly increased predicted annual available power and energy production for urban wind energy systems [11]. Fallahpour et al. (2025) [12] proposed a multi-objective optimization framework designed to enhance mass flow rate and average air velocity while simultaneously minimizing the temperature differential between indoor and outdoor environments in buildings situated in hot-arid climates. They employed iterative optimization alongside CFD simulations, demonstrating advancements in the design process [12]. In another study, Abdeen et al. (2019) [13] conducted an in-depth investigation into the optimization of solar chimney configurations as a means to enhance natural ventilation within buildings. By employing a systematic evaluation process and utilizing Ansys DesignXplorer, the researchers were able to identify design modifications that significantly improved thermal comfort and airflow performance [13]. These studies collectively demonstrate the growing relevance of DesignXplorer in architectural contexts, where it supports efficient, performance-driven decision-making in complex environmental systems.

Ansys DesignXplorer offers two approaches to optimization: direct optimization and indirect optimization. These approaches produce similar results, although they follow different procedures. Direct optimization proceeds without intermediate steps and can quickly determine the most effective solution. However, it does not provide detailed intermediate results or graphical representations of how individual or multiple parameters influence the objectives. In contrast, indirect optimization uses data generated from a response surface cell, and its accuracy depends on the precision and quality of this surface in predicting system behavior. The response surface method utilizes machine learning algorithms to create a mathematical model that can reliably estimate system performance based on changes in input parameters. Therefore, the indirect optimization method allows for immediate

Buildings 2025, 15, 4130 4 of 32

approximations of CFD results without the need to run full simulations, unlike the direct optimization approach [8] (ANSYS 2023). In this research, Ansys DesignXplorer with the indirect optimization method was employed to improve the thermal performance of the proposed biomimetic opaque ventilated façade solutions.

The optimization process integrates four interdependent components. First, the biomimetic OVF was parametrically reconstructed in Ansys SpaceClaim to enable design variable manipulation. Second, a DOE methodology was applied to strategically sample the parameter space and generate training data. Third, machine learning algorithms embedded within Ansys DesignXplorer were used to construct response surface surrogate models that predict key CFD outputs, namely inner skin surface temperature and surface area. Fourth, multi-objective optimization algorithms were applied to these surrogate models to identify optimal configurations that balance thermal efficiency with material economy.

In the present study, the surrogate models generated through DesignXplorer effectively approximate CFD outputs across thousands of design configurations, enabling comprehensive optimization without resorting to computationally expensive full CFD simulations for every iteration. This approach demonstrates a scalable, simulation-integrated method for optimizing façade systems in extreme climate conditions, combining parametric control, thermal simulation, and machine learning within a unified environment. By leveraging the synergy between bio-inspired design strategies and data-driven optimization, the study contributes a replicable and efficient methodology for advancing performance-driven façade design in architectural practice.

To explore the practical implications of the optimized design, the study also extends beyond simulation by examining its application in real-world building scenarios. The most promising façade configuration was further evaluated under varying environmental conditions and applied to low-rise commercial buildings in a hot arid climate. This application demonstrated the design's potential for real-world implementation, confirming its effectiveness in enhancing thermal performance and its adaptability to conventional construction practices.

2. Biomimetic Opaque Ventilated Façade Optimization

2.1. Parametrization Process

Any design optimization problem involves defining variables, objectives, and constraints. Variables are subsets of design parameters, while objectives define the design's goodness. Constraints are functions of design variables that define a feasible variable space. Optimization is the iterative process of altering the design space for a design that maximizes or minimizes the objectives. In this study, four input parameters were selected to minimize the two identified objectives, or output parameters, as called in the Ansys workbench system, which are reducing both the average inner skin surface temperature and the total surface area.

In the previous study conducted by Alyahya et al. (2025) [4], it was found that changes to the height and angle of the top mound had a notable effect on the average temperature of the inner skin surface. To investigate this, three CFD simulations were carried out for each selected mound height to analyze airflow behavior and performance differences. For the analysis of top mound angle configurations, four additional CFD simulations were performed using mounds with a fixed height of 30 cm. These configurations are illustrated in Figure 2 [4]. The results related to mound height showed that increasing the height from 0.3 m to 1 m led to a corresponding decrease in the average inner skin temperature. However, this temperature reduction came with an increase in the total surface area [4]. In this study, to explore the potential for reducing both the inner skin temperature and

Buildings **2025**, 15, 4130 5 of 32

the surface area, the front and back face heights of the top mound were parameterized independently. This approach aimed to determine whether adjusting one side more than the other could help balance the two performance goals. The height values for both faces were constrained between 0.1 m and 1 m. In this context, the height of the front face is referred to as "Front H," while the height of the back face is referred to as "Back H," as shown in Figure 3.

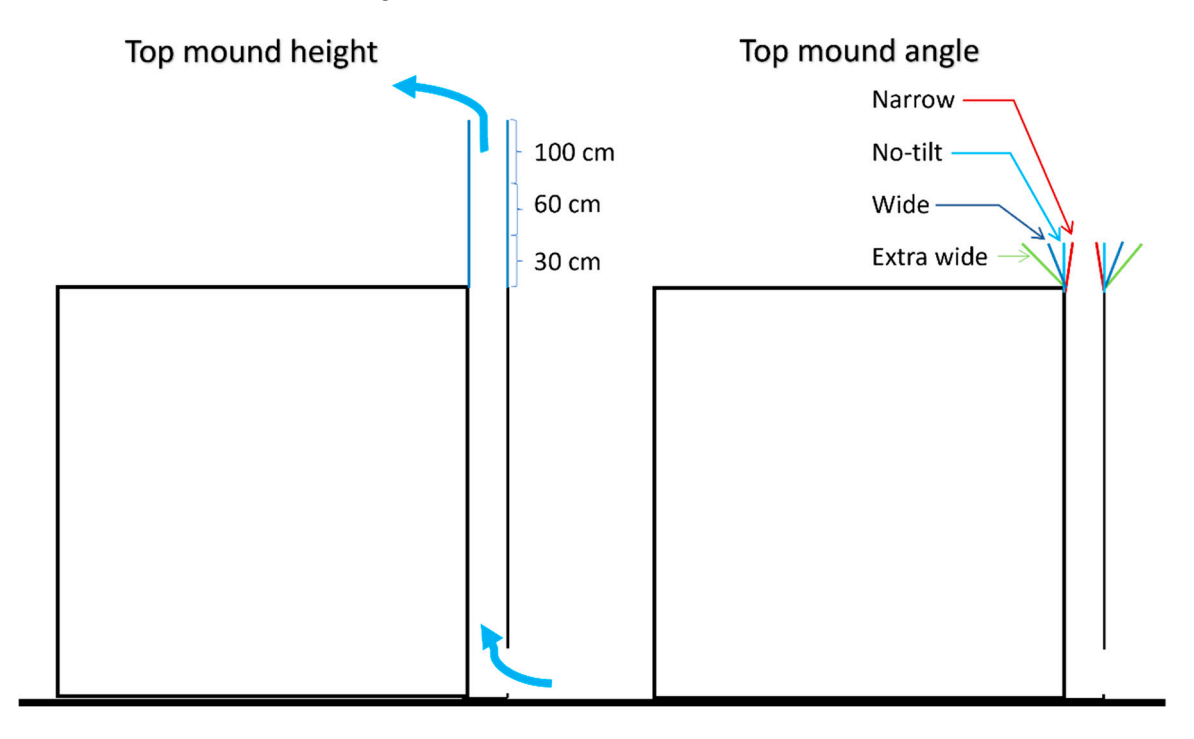


Figure 2. The tested heights and angles of the biomimetic top mound design from the previous study [4].

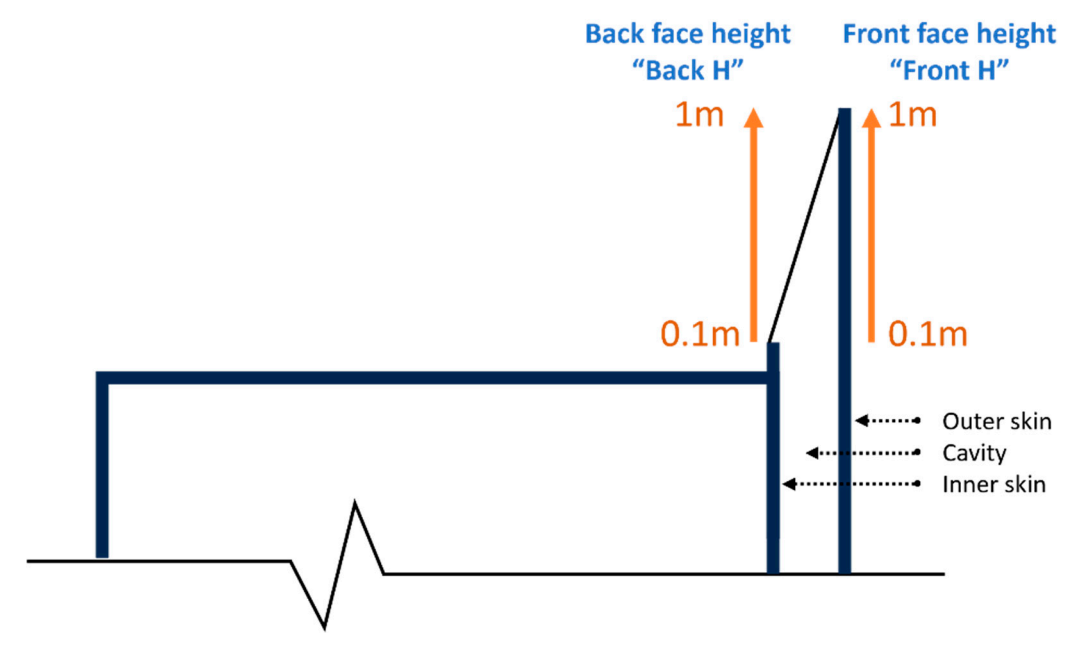


Figure 3. The height parameters of the mound's front and back faces.

With respect to the mound angle, it was previously demonstrated that the wide mound proved to be the most effective solution. However, the ideal angle that optimizes thermal performance remains uncertain, as there was a point at which the thermal performance

Buildings **2025**, 15, 4130 6 of 32

began to deteriorate with the extra-wide mound. In addition, it should be noted that the front and back sides of the mound were symmetrically expanded. So, the performance of the mound in situations where the front and back faces have varying angles has not yet been assessed. In order to parameterize the expansion of the top mound angle, the distance from zero, which represents a no-tilt mound, was increased to a distance of 0.2 m from the cavity. For instance, in the case where the parameter "Front W", which represents the measurement of the front face expansion, is set at 0.2 m, and the parameter "Back W" is set to zero, the resulting mound will exhibit no tilt in the back face and only a tilt in the front face, as displayed in Figure 4.

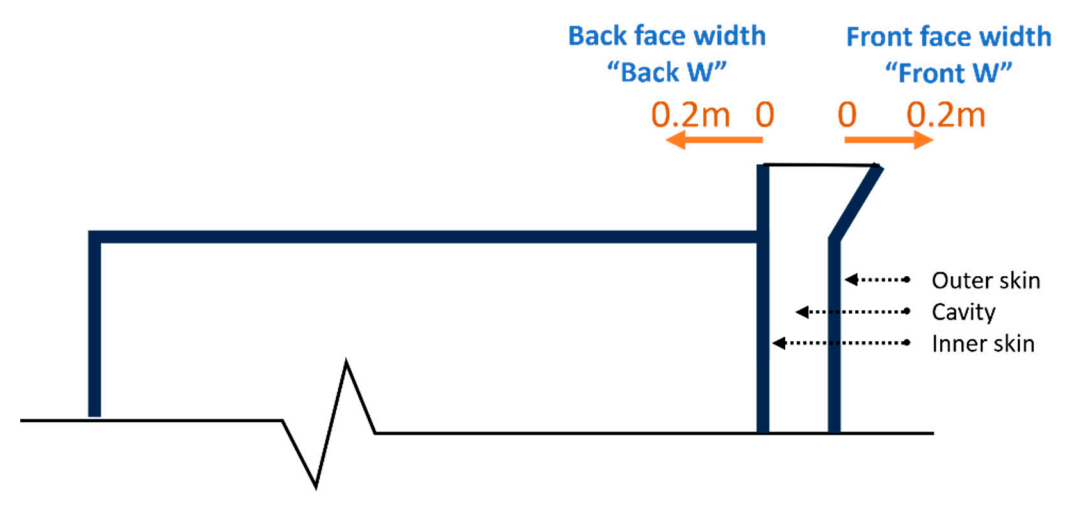


Figure 4. The expansion parameters of the mound's front and back faces.

2.2. Design of Experiments

After parametrizing the wide mound solution, the Design of Experiments (DOE) technique is employed to systematically find the placement of sampling points. In the field of engineering, there is a vast selection of different DOE algorithms and methods that can be used. They serve the aim of dividing the range of changes in variables or input parameters into different values ranging from the minimum to the maximum based on a specific pattern; these values are known as design points. Following that, a collection of these defined values, or design points, are allocated into separate rows within a table, with each row representing an individual solution. The results obtained from each solution illustrate the impact of the input parameters on the output parameters.

The default design of experiments type in Ansys is the Central Composite Design (CCD). The CCD is a robust and effective method that yields significant information regarding experimental variables and errors while requiring a limited number of experimental runs [14]. This approach incorporates a center point, points along the axis of the input parameters, and additional points selected using a fractional factorial design. The Auto-Defined design type of CCD was used as the process of design exploration involves the automatic selection of the appropriate design type, which is determined by the number of input variables. It is advisable to utilize this option in the majority of situations due to its automated switching between G-Optimality when the number of input variables is five and VIF-Optimality otherwise [8].

The DOE generated a table with 26 design points; subsequent experiments, or, in this case, CFD simulations, were conducted to obtain results for the defined targets, as seen in Table 1. The process required an extremely long time because each of the 26 defined design points had to be solved individually in order to calculate the output parameters result. The phrase "crown area" in the table represents the total surface area of the raised top mound from all four sides, without the entire surface of the opaque ventilated façade. Figure 5 is a

Buildings **2025**, 15, 4130 7 of 32

graph demonstrating the relationship between design points and output parameters. Each design point on the lower horizontal *x*-axis is accompanied by a range of values on the right and left y-axes, which reflect the inner skin surface temperature and crown area.

Table 1. The design points generated during DOE.

Design Points of Design of Experiments						
Input Parameters					Output Para	meters
Design Points	Back H (m)	Back W (m)	Front H (m)	Front W (m)	Average Inner Skin Surface Temperature (°C)	Crown Area (m ²)
1	0.55	0.1	0.55	0.1	54.33	3.68
2	0.1	0.1	0.55	0.1	54.36	2.30
3	1	0.1	0.55	0.1	55.07	5.16
4	0.55	0	0.55	0.1	54.33	3.60
5	0.55	0.2	0.55	0.1	54.27	3.82
6	0.55	0.1	0.1	0.1	56.31	2.30
7	0.55	0.1	1	0.1	54.08	5.16
8	0.55	0.1	0.55	0	54.35	3.60
9	0.55	0.1	0.55	0.2	54.28	3.82
10	0.233	0.030	0.233	0.030	54.72	1.52
12	0.233	0.170	0.233	0.030	54.66	1.71
13	0.867	0.170	0.233	0.030	56.18	3.64
14	0.233	0.030	0.867	0.030	54.25	3.56
15	0.867	0.030	0.867	0.030	54.30	5.60
16	0.233	0.170	0.867	0.030	54.22	3.84
17	0.867	0.170	0.867	0.030	54.15	5.77
18	0.233	0.030	0.233	0.170	55.44	1.71
19	0.867	0.030	0.233	0.170	56.84	3.84
20	0.233	0.170	0.233	0.170	55.47	1.91
21	0.867	0.170	0.233	0.170	56.32	3.92
22	0.233	0.030	0.867	0.170	54.16	3.64
23	0.867	0.030	0.867	0.170	54.18	5.77
24	0.233	0.170	0.867	0.170	54.24	3.92
25	0.982	0.006	0.150	0.002	58.33	3.63
26	0.993	0.192	0.966	0.192	54.13	6.76

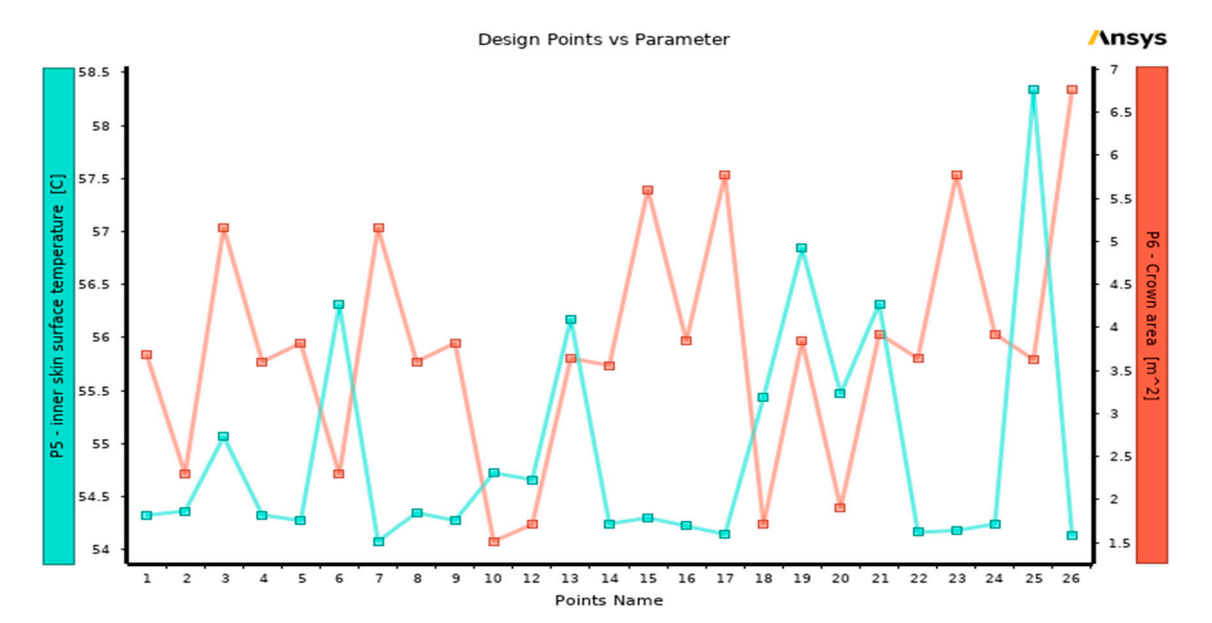


Figure 5. DOE Design points vs. output parameters.

Buildings 2025, 15, 4130 8 of 32

2.3. Response Surfaces

The next step to perform the optimization process after the DOE is to use the response surface method. The response surface method uses machine learning algorithms for obtaining a mathematical function that is capable of accurately predicting the behavior of a system as a result of variations in its input parameters. Without performing a full solution, it instantly provides approximations of the output parameters throughout the design space based on the results of the 26 design points that were generated during the DOE step. The accuracy of a response surface is dependent upon several factors, including the complexity of the variables in the solution, the number of points in the initial DOE table, and the type of response surface employed. When it comes to the response surface type, the genetic aggregation algorithm is the one that is used by default. In this research, the genetic aggregation algorithm was employed because it is an automated method that selects, customizes, and generates the best suitable response surface for each output parameter. It is important to note that the machine learning capabilities used in this study are based on the built-in surrogate modeling tools provided by Ansys DesignXplorer. These tools employ automated algorithms, such as the genetic aggregation method, to generate response surface models from the DOE data. However, Ansys does not provide detailed access to the internal structure of the machine learning models or training metrics. As a result, information such as root mean square error (RMSE), training versus testing performance, number of epochs, or hyperparameter tuning processes is not available to the user. In this context, the machine learning functionality serves as a streamlined and efficient means of accelerating CFD-driven design exploration, rather than a fully customizable or transparent machine learning framework.

After generating the response surface, the goodness of fit for each output parameter was evaluated to determine whether the answer was satisfactory. The results demonstrated a reasonable correlation between the predicted values and the simulated design points; however, the maximum predicted error value of the average inner skin surface temperature was $0.5\,^{\circ}$ C, which is greater than what was expected. As a result, additional simulations were carried out by making refinement points, which are design points added to enrich and improve the predicted values of the response surface.

Automatically, refinement points are added, and when each point is completely solved, the maximum predicted error value is updated until each output parameter's tolerance value is met. For the average inner skin surface temperature and the crown surface area, the identified tolerance value target was set at $0.3\,^{\circ}\text{C}$ and $0.1\,\text{m}^2$, respectively. As shown in Figure 6 and Table 2, the refinement process created seven design points until the target was reached with maximum predicted error values of the average inner skin surface temperature and the crown area of $0.24\,^{\circ}\text{C}$ and $0.03\,\text{m}^2$, respectively. As a result, Figure 7 demonstrates how the predicted and observed points are in excellent agreement, indicating that it is possible to assume that the data obtained would provide the best values possible for each output parameter based on the inputs.

Selecting Min-Max search in the Outline pane after the response surface has been updated displays the sample points, which represent the minimum and maximum values determined for each output parameter in the response surface database. The Min-Max search algorithm analyzes the complete range of output parameters inside the response surface in order to estimate the minimum and maximum values associated with each parameter. Within the design space, there is a variation of 5.08 °C between the lowest possible average inner skin surface temperature and the highest possible temperature. Regarding the crown area, the difference is 6.27 m² between the smallest and largest possible designs, as displayed in Table 3. Both output parameters have large ranges, but the crown area is exceptionally extreme, with a range of more than 10 times the area of

Buildings 2025, 15, 4130 9 of 32

the minimum design point. Thus, finding the trade-off between the output parameters to achieve the correct balance is very important in this study.

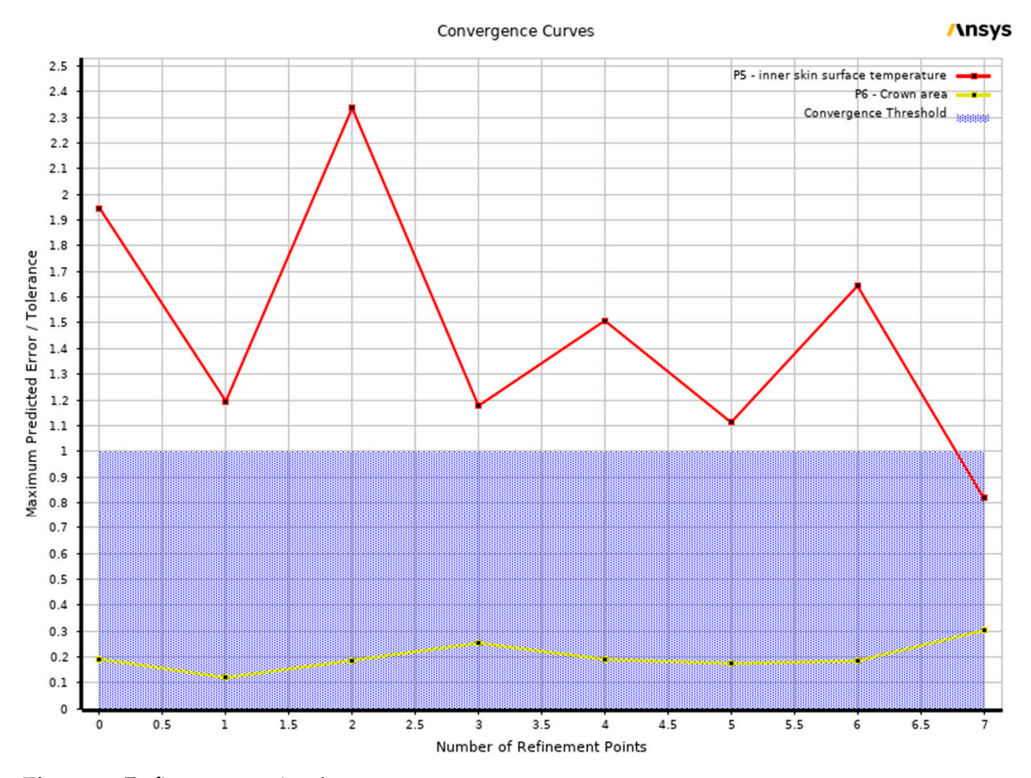


Figure 6. Refinement points' convergence curves.

Table 2. The generated refinement points data.

	Refinement Points						
		Output Parameters					
Design Points	Back H (m)	Back W (m)	Front H (m)	Front W (m)	Average Inner Skin Surface Temperature (°C)	Crown Area (m²)	
1	1	0.14	0.1	0.07	57.59	3.71	
2	0.57	0	0.1	0	57.59	2.15	
3	0.9	0.09	0.38	0.2	55.51	4.50	
4	0.41	0	0.1	0.1	56.26	1.81	
5	0.1	0	0.1	0	55.46	0.64	
6	0.59	0.11	0.1	0	56.76	2.25	
7	0.24	0.2	0.1	0.08	55.51	1.43	

 Table 3. The estimated minimum and maximum values of each output parameter.

			Min-Max Search			
Name	Back H (m)	Back W (m)	Front H (m)	Front W (m)	Average Inner Skin Surface Temperature (°C)	Crown Area (m²)
		Out	put parameter mini	mums		
Average inner skin surface temperature	0.4	0	0.77	0.1	53.85	3.82
Crown area	0.1	0	0.1	0	55.46	0.64
		Out	put parameter max	mums		
Average inner skin surface temperature	1	0	0.1	0	58.93	3.53
Crown area	1	0.2	1	0.2	54.2	6.91

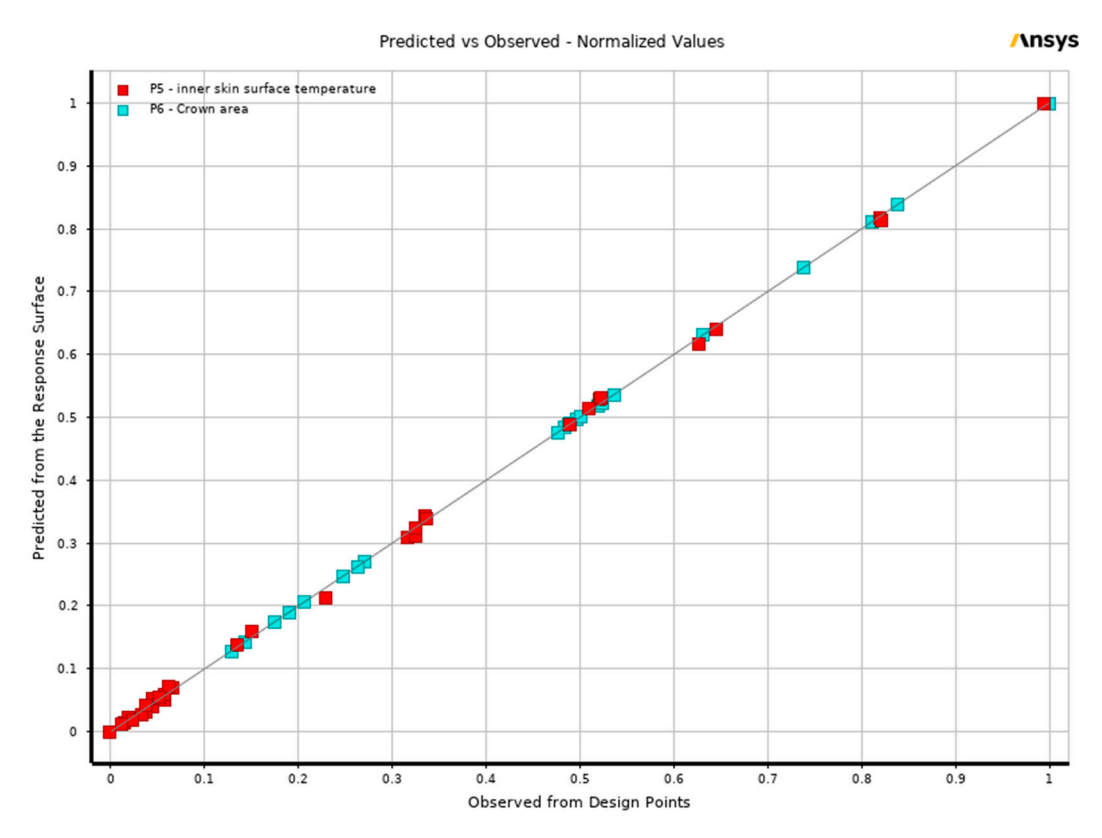


Figure 7. Goodness of fit diagram for the output parameters.

The design space can be explored more easily with response surface charts, which show visually how different parameters affect each other. There are four charts available: the Spider chart, the Response chart, the Local Sensitivity chart, and the Local Sensitivity Curves chart. When a response surface is modified, one response point and one of each chart type are automatically generated. There is no limit to the number of response points and charts that can be explored. To begin understanding and exploring the effect of parameters on one another, the response point was set to the same dimensions as the original wide mound solution, which is 0.3 m for front and back height and 0.07 m for front and back width.

The response surface charts generated in response to the original wide mound design point reveal some interesting findings. Regarding the back height, both the inner skin surface temperature and the crown area indicate that in order to minimize them, the height of the back face should not exceed 0.2 m, as can be seen in Figure 8, which displays two-dimensional contour graphs that provide a visual representation of the impact of changes in the back height parameter on each output parameter. Consequently, in the next optimization step, the allowable range of values for the back face height parameter is limited to 0.1 m to 0.2 m, rather than 1 m. The design space range is kept the same for the optimization step for the back width and front height parameters since these parameters demonstrate an opposite influence between the output parameters, which means minimizing one output parameter leads to maximizing the other, as illustrated in Figures 9 and 10. Regarding the front width parameter, the range is constrained to be between 0 and 0.04 m, as the minimal values for both output parameters fell within this range, as displayed in Figure 11.

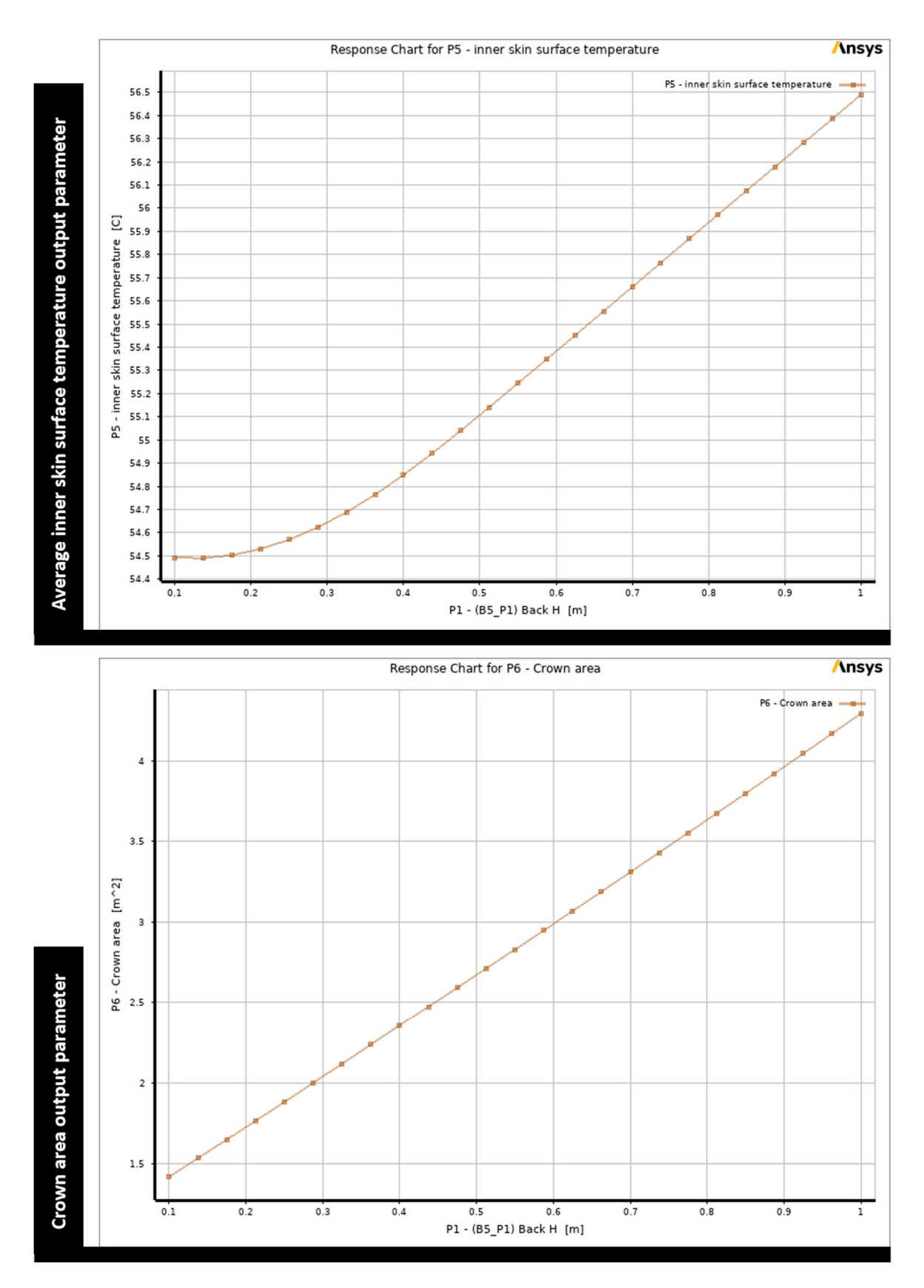


Figure 8. Two-dimensional graphs of the impact of changes in Back H parameter.

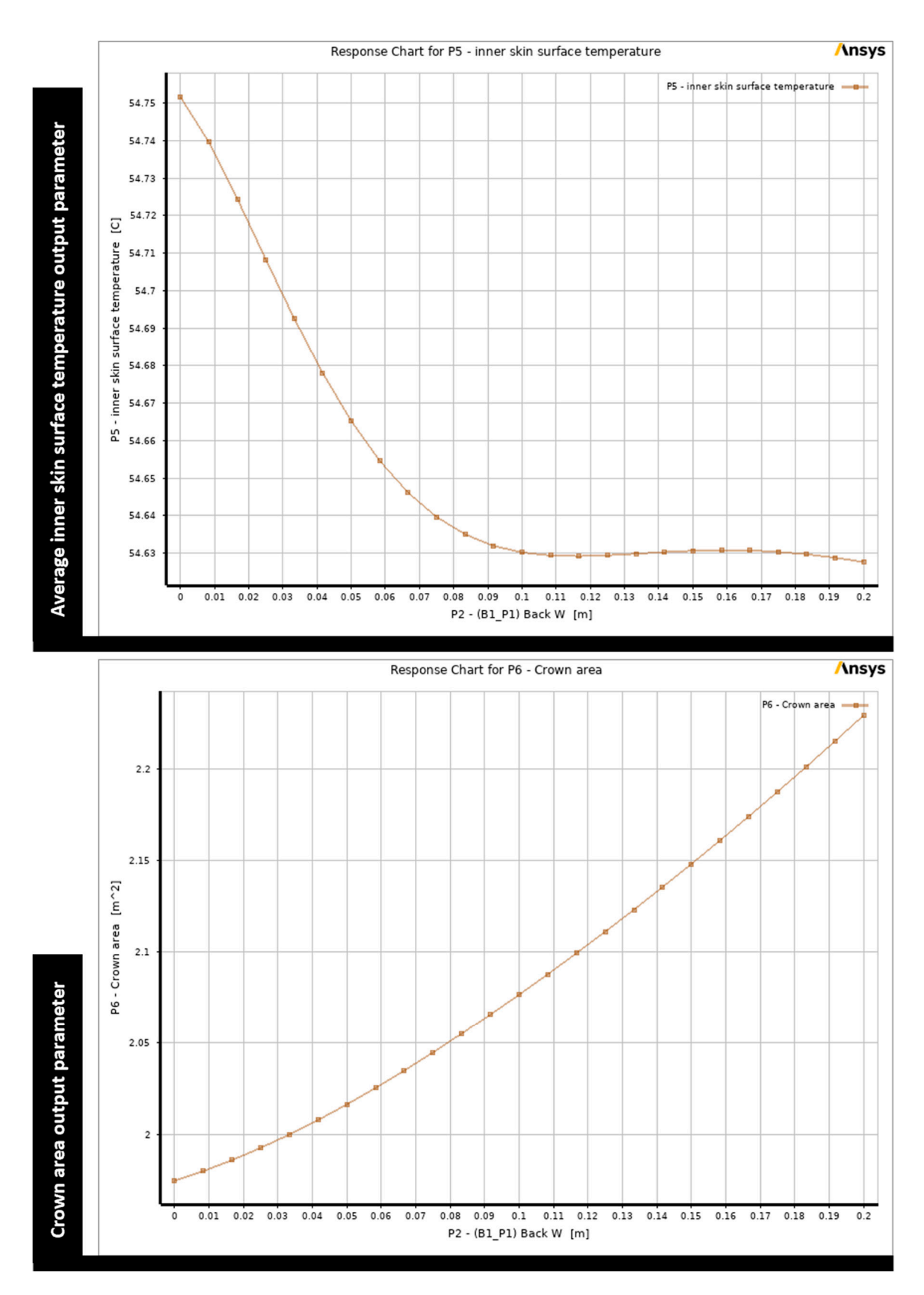
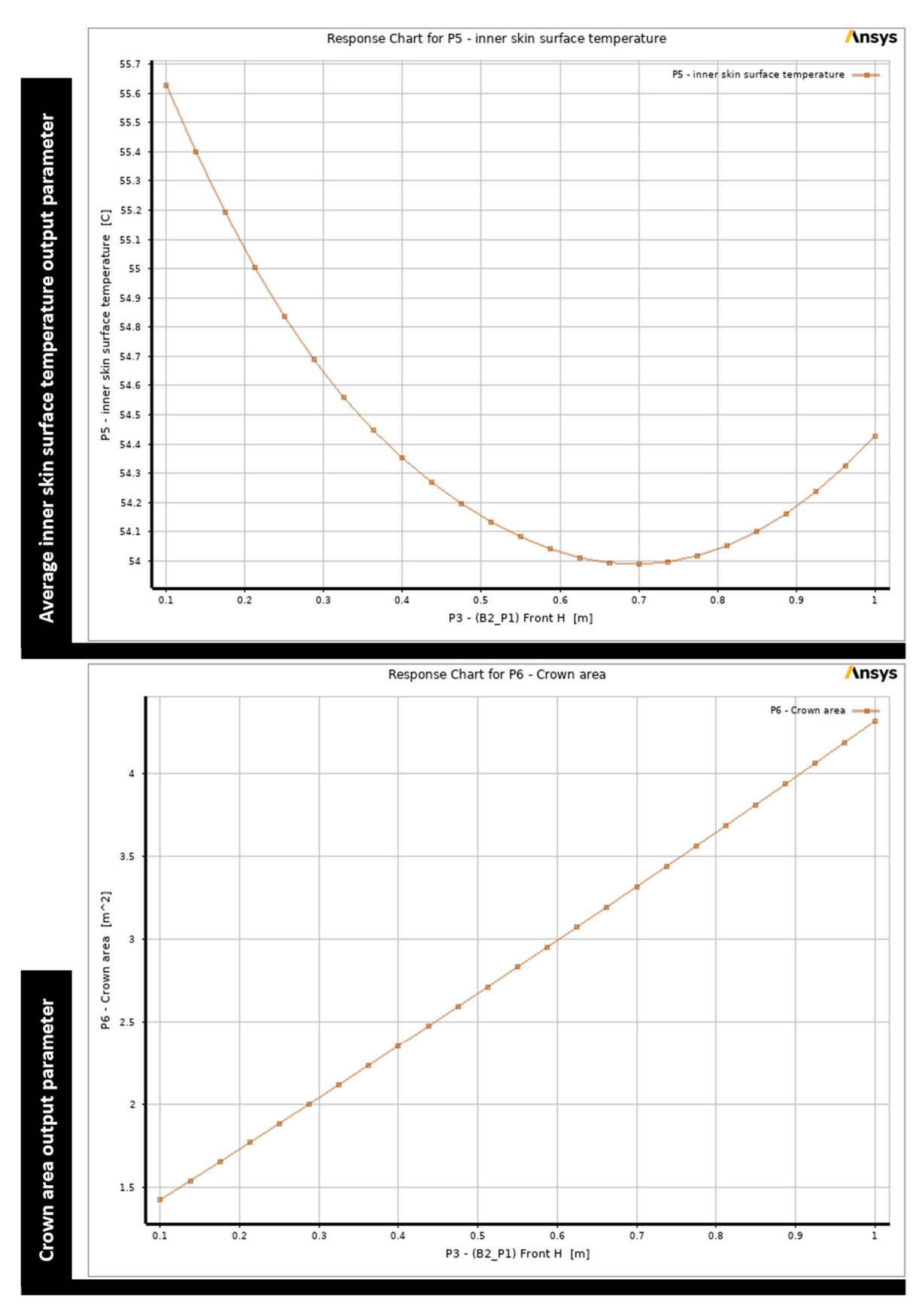


Figure 9. Two-dimensional graphs of the impact of changes in Back W parameter.

Buildings 2025, 15, 4130 13 of 32



 $\textbf{Figure 10.} \ \textbf{Two-dimensional graphs of the impact of changes in Front H parameter.}$

Buildings 2025, 15, 4130 14 of 32

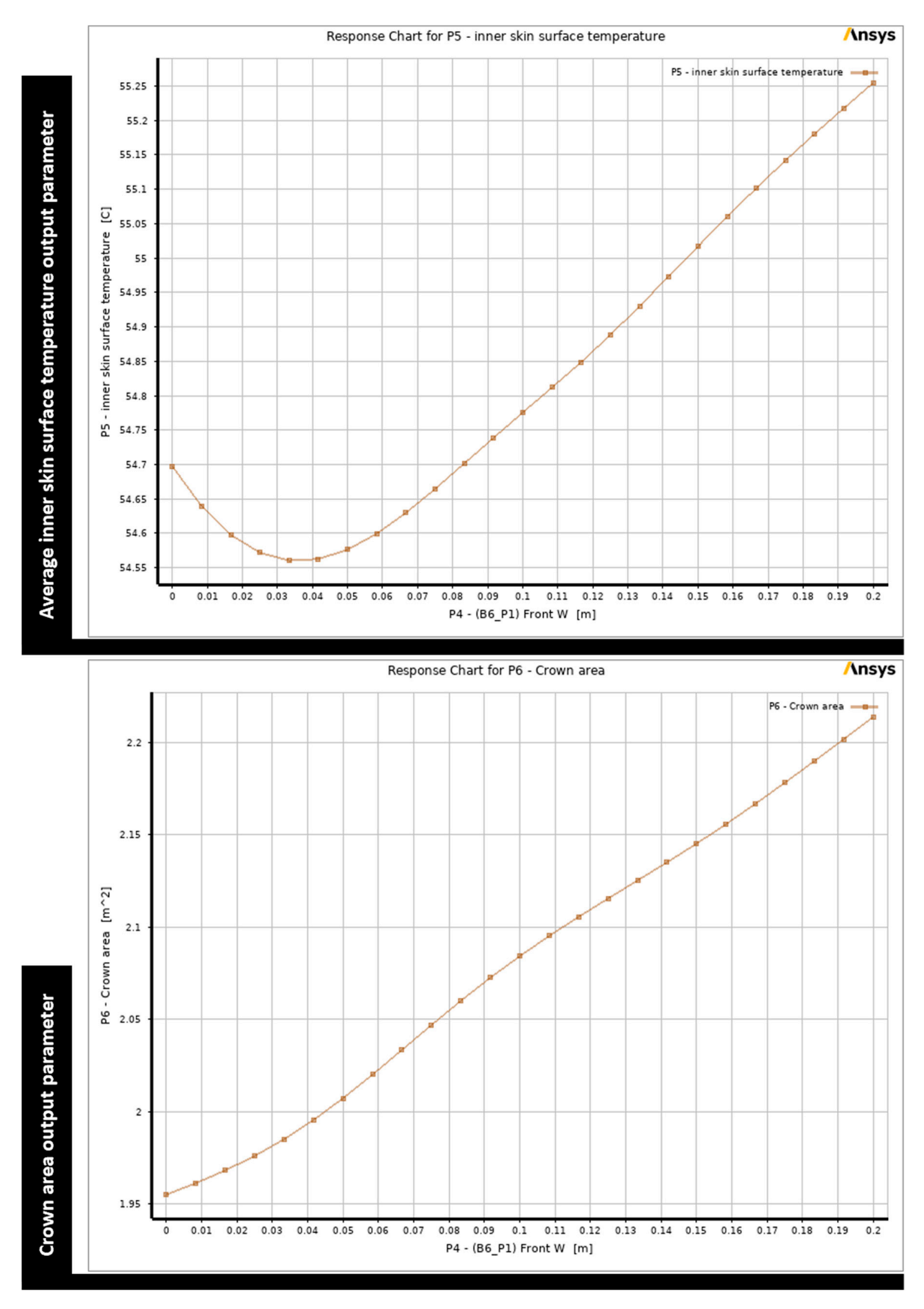


Figure 11. Two-dimensional graphs of the impact of changes in Front W parameter.

Buildings 2025, 15, 4130 15 of 32

2.4. Goal-Driven Optimization

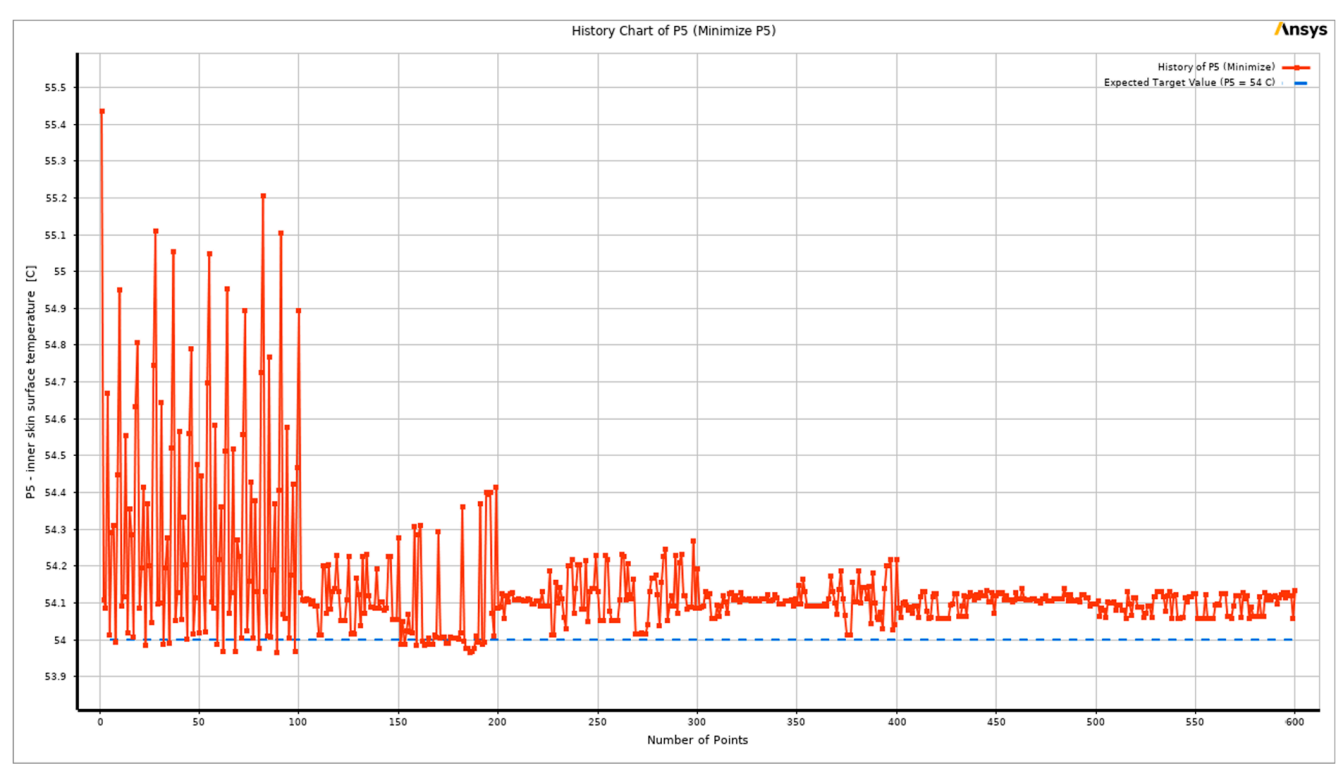
Goal-driven optimization refers to a combination of strategies used to optimize several objectives while considering constraints. These techniques aim to identify the most optimal designs from a given sample set, based on predefined goals established for the parameters. Response surface optimization and direct optimization are two different types of goal-driven optimization methods that DesignXplorer provides. A response surface optimization system relies on the data from its own response surface cell, and hence its performance is dependent upon the accuracy and quality of the response surface. Screening, Multi-Objective Genetic Algorithm (MOGA), Nonlinear Programming by Quadratic Lagrangian (NLPQL), and Mixed-Integer Sequential Quadratic Programming (MISQP) are the optimization methods that can be used in Ansys [8]. These optimization techniques all make use of response surface assessments rather than real solves, as is the case in the direct optimization system.

Due to the presence of two objectives or output parameters in this study, only screening and multi-objective genetic algorithm methods are applicable. Screening is commonly employed to identify an initial set of candidate points for a preliminary design; however, a multi-objective genetic algorithm offers a more sophisticated approach compared to the screening method [8]. Hence, the optimization is carried out using the multi-objective genetic algorithm approach. The multi-objective genetic algorithm employed in goal-driven optimization is a hybrid adaptation of the well-known NSGA-II (Non-dominated Sorted Genetic Algorithm-II) that incorporates controlled elitism principles.

The process of the multi-objective genetic algorithm begins by using the initial population. The second step comes after the first iteration. Each population is run and generates a new population through cross-over and mutation until it meets the number of samples set by the property for the number of samples per iteration. The third step involves updating the design points in the new population. In the fourth step, the optimization is validated to make sure it has converged, and this can be performed by either achieving the allowable Pareto percentage or the convergence stability percentage. If the previous conditions are not met, the procedure proceeds to the fifth step, in which the optimization is assessed to determine if it satisfies the specified stopping criterion. If the task for the maximum number of iterations is met, the procedure is halted before achieving convergence. If not, the procedure iterates steps 2 through 5 and produces a new population until convergence or the specified stopping criteria are achieved. In this study, the number of initial samples, the number of samples per iteration, the maximum allowable Pareto percentage, the convergence stability percentage, and the maximum number of iterations are set to the default value to avoid the process converging prematurely.

To find optimal designs, the optimization cell of a goal-driven optimization system requires the specification of design goals in the form of objectives and constraints. The objective type of both output parameters has been specified to be minimized with a target that is lower than the initial wide mound solution. The target average temperature for the inner skin surface was set at $54.0~^{\circ}$ C, while the area of the crown was set at $1.2~^{\circ}$ C with no constraints. Due to the use of response surface evaluations rather than actual solutions, the optimization procedure took only a few seconds to reveal the results. The optimization process converged after 543 evaluations. Figure 12 represents the evolution of the population of these 543 evaluation points during the iterations of the optimization for each output parameter until it converged, whereas Figures 13 and 14 exhibit the evolution of the population for each input parameter.

Buildings 2025, 15, 4130 16 of 32



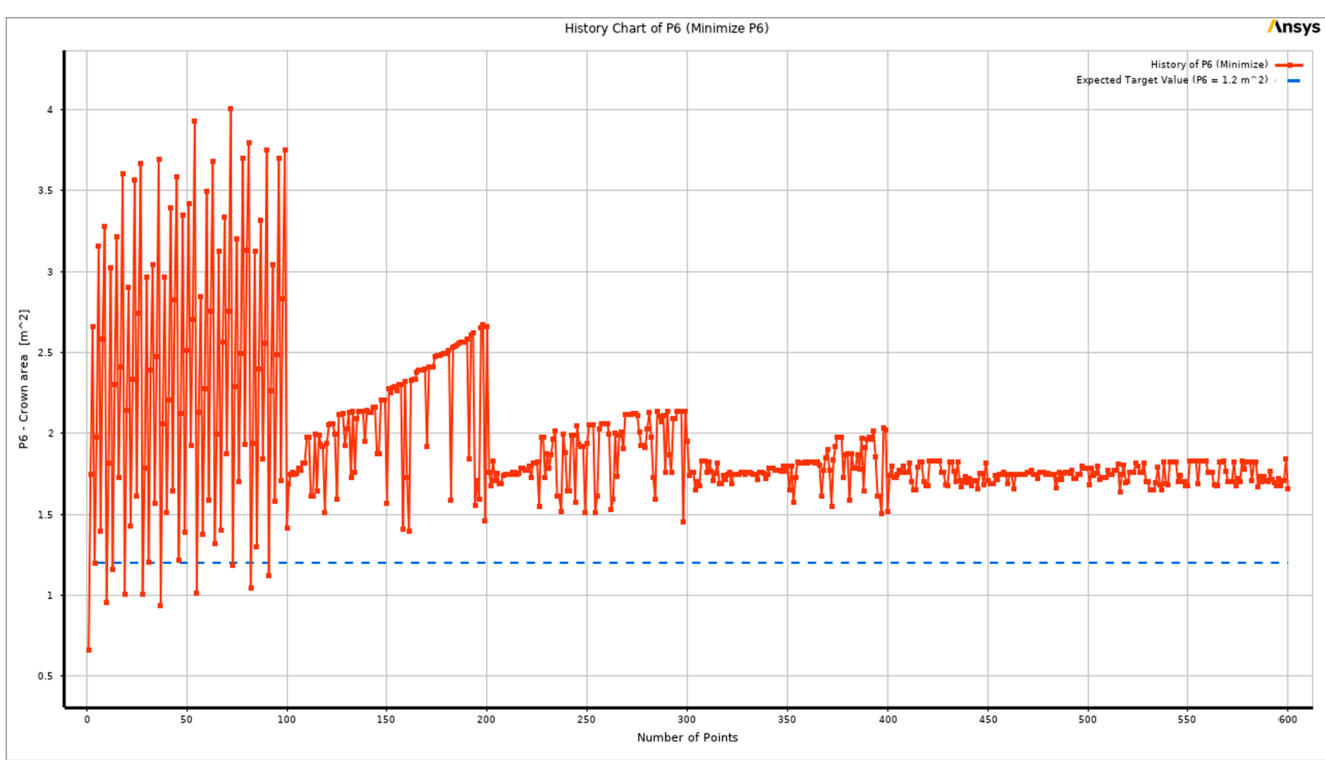


Figure 12. The population evolution history charts for output parameters.

Buildings 2025, 15, 4130 17 of 32

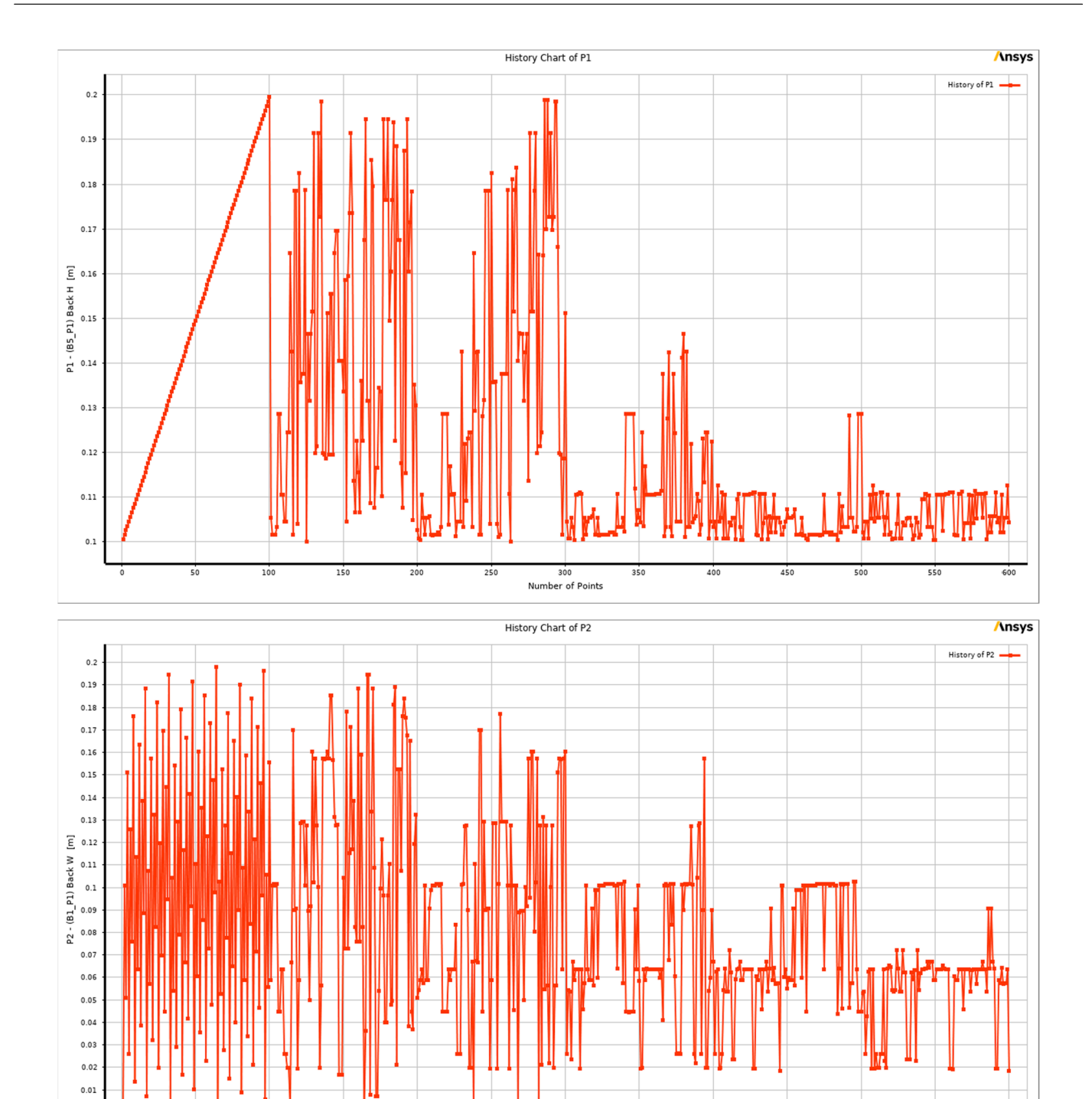


Figure 13. The population evolution history charts for Back H and Back W parameters.

300 Number of Points

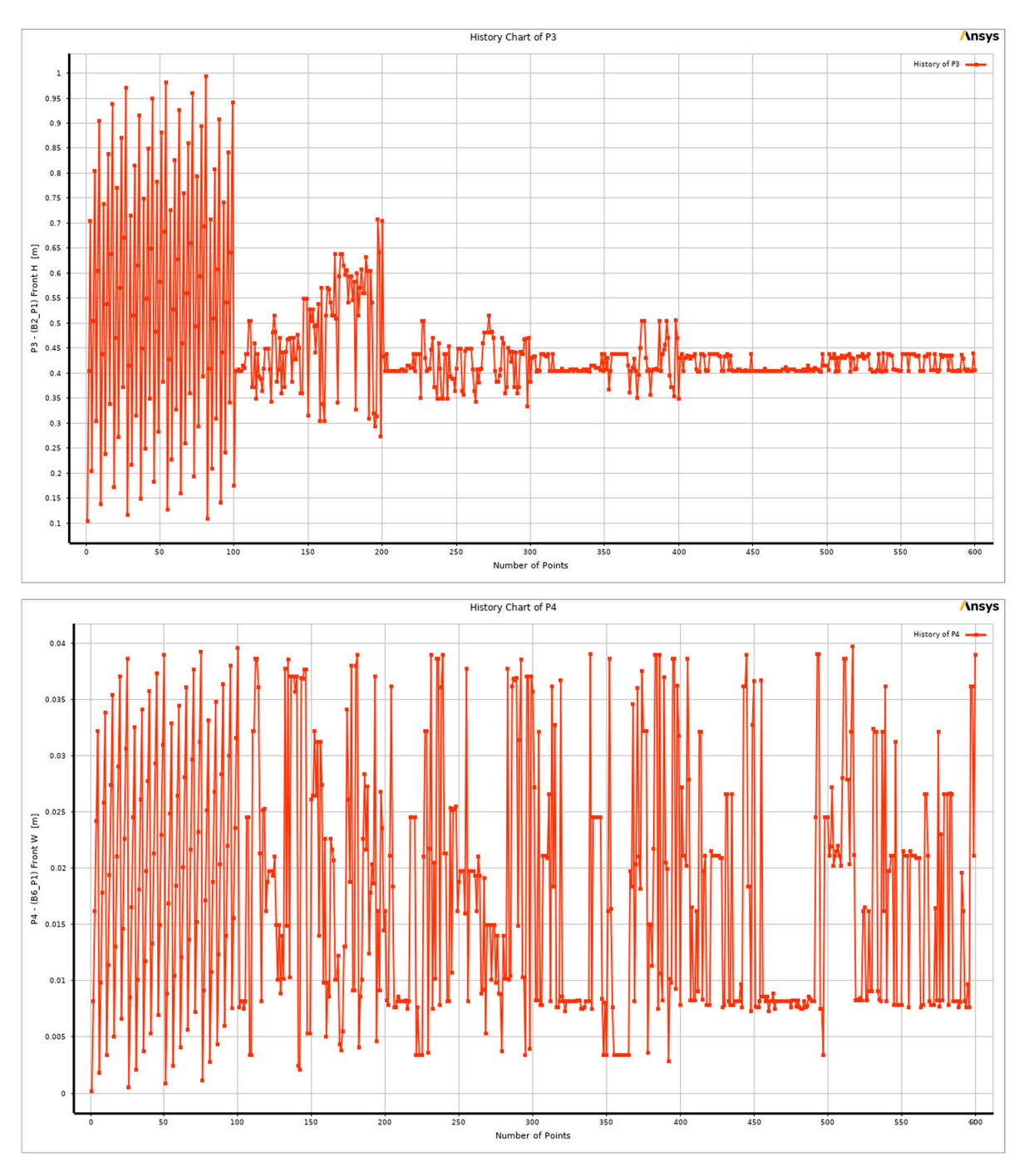


Figure 14. The population evolution history charts for Front H and Front W parameters.

The optimization process revealed the three most optimal candidate points, as illustrated in Figure 15. The candidate points share common values with many design points, as demonstrated in the trade-off chart and the samples chart of the last iteration in Figure 16. However, the forms of all these points are nearly identical. When compared to the initial solution of a wide mound, all of the candidate points that were found show outcomes that are better in both objectives. The average temperature differential on the inner skin surface was approximately $0.4~^{\circ}$ C, whereas the crown area had a difference of about $0.3~\text{m}^2$. The outcome is satisfactory; however, it would be ideal to investigate other possibilities that, at one point in time, cause the optimization process to give more significance to the target of the average inner skin surface temperature and, at another point in time, to the objective of the crown area.

Buildings 2025, 15, 4130 19 of 32

Table of Schematic C4: Optimization						
	A	В	С	D		
1	■ Optimization Study					
2	Minimize P5 Goal, Minimize P5 (Default importance)					
3	Minimize P6	Goal, Minimize P6 (Defa	ult importance)			
4	■ Optimization Method					
5	The MOGA method (Multi-Objective Genetic Algorithm) is a variant of the popular NSGA-II (Non-dominated Sorted Genetic Algorithm-II) based on controlled elitism concepts. It supports multiple objectives and constraints and aims at finding the global optimum.					
6	Configuration	Generate 100 samples initially, 100 samples per iteration and find 3 candidates in a maximum of 20 iterations.				
7	Status	Converged after 543 e	valuations.			
8	□ Candidate Points					
9		Candidate Point 1	Candidate Point 2	Candidate Point 3		
10	P1 - (B5_P1) Back H (m)	0.10444	0.10454	0.10197		
11	P2 - (B1_P1) Back W (m)	0.026	0.042591	0.053119		
12	P3 - (B2_P1) Front H (m)	0.4306	0.4306	0.40539		
13	P4 - (B6_P1) Front W (m)	0.027185	0.020236	0.021068		
14	P5 - inner skin surface temperature (C)	54.087	54.079	54.104		
15	P6 - Crown area (m^2)	★★ 1.7378	★★ 1.7553	★★ 1.6823		

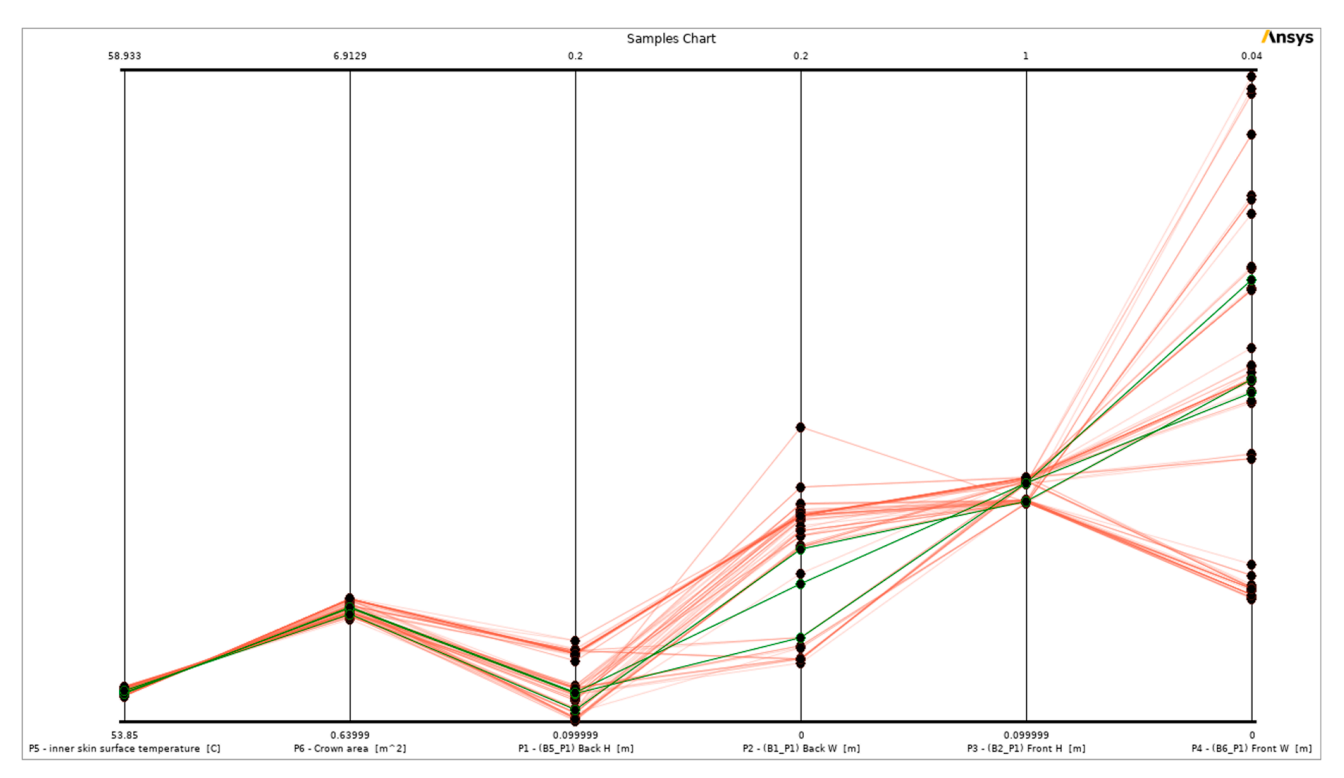
Figure 15. The first candidate points (the number of gold stars indicate how well the parameter meets the stated objective).

In the Min-Max search of the response surfaces, the minimum average inner skin surface temperature achievable is $53.85\,^{\circ}$ C, and the minimum crown area is $0.64\,^{\circ}$ C. Consequently, the first optimization target was set to reach $53.85\,^{\circ}$ C, and the crown area target was set to $2\,^{\circ}$ m², which is the same as the original wide mound solution. The second time, the target was the opposite, with the average inner skin surface temperature set to $54.4\,^{\circ}$ C and the crown area target set to $0.64\,^{\circ}$ m². Figure 17 displays the candidate points of this optimization that prioritize the objective of the average inner skin surface temperature. The results indicate that the temperature difference on the average inner skin surface is less than $0.1\,^{\circ}$ C compared to the initial optimization, which is quite insignificant. Furthermore, the crown area has risen by around $0.2\,^{\circ}$ m². As a result, these candidate points were not considered as optimal solutions.

Figure 18 illustrates the candidate points of the optimization that prioritize the crown area, revealing a noteworthy finding. This round of optimization resulted in a crown area that is $1.3\,\mathrm{m}^2$ rather than $1.7\,\mathrm{m}^2$ in the earlier optimization, and it is $0.7\,\mathrm{m}^2$ less than the wide mound solution in the initial phase. Simultaneously, the inner skin surface temperature drops by $0.1\,\mathrm{^\circ C}$ as compared to the initial wide mound solution.

All of these optimizations demonstrate a significant decrease in the average inner skin surface temperature, particularly in the first optimization, where it achieved a level that was only around $0.15\,^{\circ}\text{C}$ higher than the minimum achievable average temperature for the inner skin surface. On the other hand, the crown area in the best scenario for optimizing it still has a difference of around $0.7\,\text{m}^2$ when compared to the minimal value that is reachable. Therefore, a constraint was placed on the target of the crown area, requiring the optimization to identify design points that are less than the specified upper bound of $1\,\text{m}^2$. Afterwards, the optimization process was updated. This optimization approach resulted in the identification of certain potential points that have half of the total area of the original

crown and lead to an only 0.3 $^{\circ}$ C rise in the average temperature of the inner skin surface, as illustrated in Figure 19.



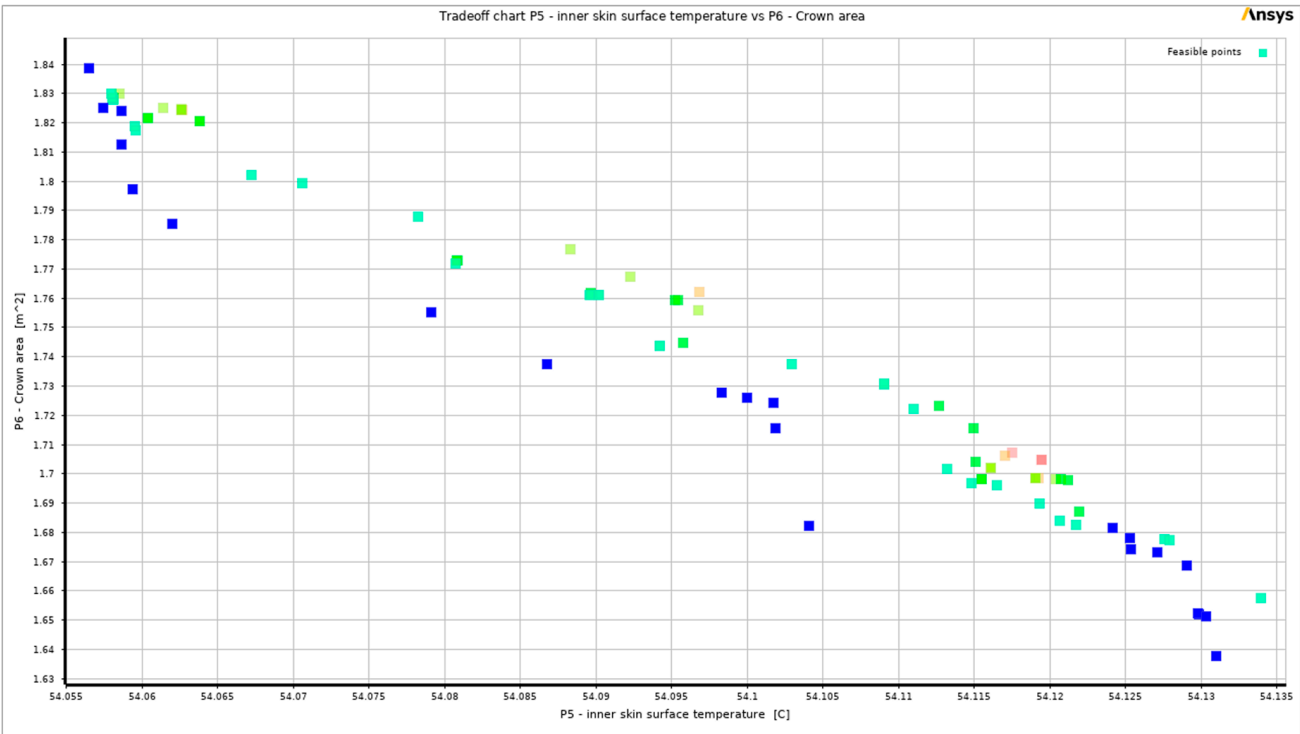


Figure 16. The samples chart (top) and the trade-off chart (bottom).

Table of	Table of Schematic C4: Optimization					
	A	В	С	D		
1	Optimization Study					
2	Minimize P5	Goal, Minimize P5 (Defa	ult importance)			
3	Minimize P6	Goal, Minimize P6 (Defa	ult importance)			
4	■ Optimization Method					
5	The MOGA method (Multi-Objective Genetic Algorithm) is a variant of the popular NSGA-II (Non-dominated Sorted Genetic Algorithm-II) based on controlled elitism concepts. It supports multiple objectives and constraints and aims at finding the global optimum.					
6	Configuration	Generate 100 samples initially, 100 samples per iteration and find 3 candidates in a maximum of 20 iterations.				
7	Status	Converged after 732 e	valuations.			
8	■ Candidate Points					
9		Candidate Point 1	Candidate Point 2	Candidate Point 3		
10	P1 - (B5_P1) Back H (m)	0.10448	0.1009	0.10101		
11	P2 - (B1_P1) Back W (m)	0.012858	0.026	0.017653		
12	P3 - (B2_P1) Front H (m)	0.5045	0.5045	0.48186		
13	P4 - (B6_P1) Front W (m)	0.032242	0.030066	0.0322		
14	P5 - inner skin surface temperature (C)	54.008	54.012	54.03		
15	P6 - Crown area (m^2)	1.9612	1.9657	1.8844		

Figure 17. The candidate points of the optimization that prioritize the objective of the average inner skin surface temperature (the number of gold stars indicate how well the parameter meets the stated objective).

Table of Schematic C4: Optimization						
	A	В	С	D		
1	■ Optimization Study					
2	Minimize P5 Goal, Minimize P5 (Default importance)					
3	Minimize P6	Goal, Minimize P6 (Defa	ult importance)			
4	■ Optimization Method					
5	The MOGA method (Multi-Objective Genetic Algorithm) is a variant of the popular NSGA-II (Non-dominated Sorted Genetic Algorithm-II) based on controlled elitism concepts. It supports multiple objectives and constraints and aims at finding the global optimum.					
6	Configuration	Configuration Generate 100 samples initially, 100 samples per iteration and find 3 candidates in a maximum of 20 iterations.				
7	Status	Converged after 636 e	valuations.			
8	■ Candidate Points					
9		Candidate Point 1	Candidate Point 2	Candidate Point 3		
10	P1 - (B5_P1) Back H (m)	0.10019	0.10109	0.10114		
11	P2 - (B1_P1) Back W (m)	0.044073	0.076202	0.071159		
12	P3 - (B2_P1) Front H (m)	0.30339	0.29337	0.29568		
13	P4 - (B6_P1) Front W (m)	0.0098993	0.0084373	0.0098		
14	P5 - inner skin surface temperature (C)	54.35	54.342	54.335		
15	P6 - Crown area (m^2)	★★ 1.3295	★★ 1.3441	★★ 1.3451		

Figure 18. The candidate points of the optimization that prioritize the objective of the crown area (the number of gold stars indicates how well the parameter meets the stated objective).

Table of Schematic C4: Optimization						
	A	В	С	D		
1	■ Optimization Study					
2	Minimize P6; P6 <= 1 m^2	Minimize P6; P6 <= 1 m^2 Goal, Minimize P6 (Default importance); Strict Constraint, P6 values less than or equals to 1 m^2 (Default importance)				
3	Minimize P5	Goal, Minimize P5 (Defa	ult importance)			
4	■ Optimization Method					
5	MOGA	The MOGA method (Multi-Objective Genetic Algorithm) is a variant of the popular NSGA-II (Non-dominated Sorted Genetic Algorithm-II) based on controlled elitism concepts. It supports multiple objectives and constraints and aims at finding the global optimum.				
6	Configuration	Generate 100 samples initially, 100 samples per iteration and find 3 candidates in a maximum of 20 iterations.				
7	Status	Converged after 732 evaluations.				
8	■ Candidate Points					
9		Candidate Point 1	Candidate Point 2	Candidate Point 3		
10	P1 - (B5_P1) Back H (m)	0.1065	0.10776	0.1065		
11	P2 - (B1_P1) Back W (m)	0.05725	0.05725	0.057295		
12	P3 - (B2_P1) Front H (m)	0.18552	0.18448	0.18445		
13	P4 - (B6_P1) Front W (m)	0.019088	0.018388	0.011214		
14	P5 - inner skin surface temperature (C)	54.733	54.739	54.757		
15	P6 - Crown area (m^2)	- 1.0002	- 0.99995	- 0.98916		

Figure 19. The candidate points of the optimization that prioritize the objective of the crown area with constraint (the number of gold stars indicates how well the parameter meets the stated objective).

The following candidate points were chosen as the best options as a result of all these optimizations for the wide mound solution. The first design point achieved an inner skin surface temperature of 54° C and a crown area of 1.7 m², which prioritizes the average inner skin surface temperature objective. The second optimal solution prioritizes minimizing the crown area and achieves a 54.7° C average inner skin surface temperature and a 0.9 m² crown area. Both optimal solutions were verified by conducting real CFD solutions with geometric dimensions that were approximated to two decimal places. These are the measurements of the first optimal solution, which is called the larger: 0.1 m for the back height, 0.05 m for the back width, 0.42 m for the front height, and 0.02 m for the front width. The second optimal solution, which is called the smaller, has dimensions of 0.1 m for the back height, 0.05 m for the back width, 0.18 m for the front height, and 0.01 m for the front width.

The larger optimal wide mound solution, when calculated with real CFD simulation, shows a little higher average inner skin surface temperature than predicted in the final results. The average inner skin surface temperature was $54.3\,^{\circ}$ C, whereas the crown area remained the same at $1.7\,\mathrm{m}^2$. On the other hand, the outcome of the actual CFD simulation of the smaller optimal wide mound solution is almost the same as the one that was expected, which was $54.8\,^{\circ}$ C for the average temperature of the inner skin surface and $0.9\,\mathrm{m}^2$ for the area of the crown. Figure 20 displays a visual comparison between the final two optimal wide mound solutions.

Buildings 2025, 15, 4130 23 of 32

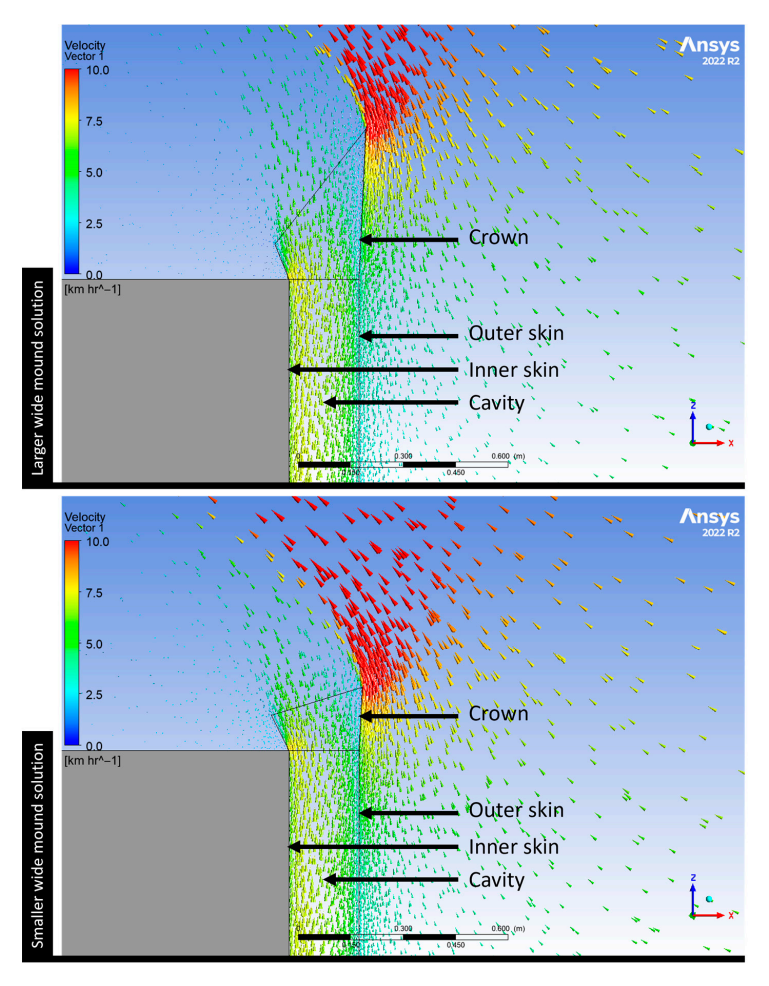


Figure 20. The optimal wide mound solutions.

3. The Optimal Solution Application

3.1. Solutions Comparison

During the parametric optimization process, two optimal solutions were identified for the wide mound façade design. To determine which of the two offered the best balance between reducing façade surface area and lowering the average temperature of the inner skin, additional CFD simulation scenarios were conducted. These simulations replicated the conditions previously applied to the baseline and unventilated façades in the author's previous study [3], including variations in wind velocity, wind direction, and solar exposure. The aim was to evaluate performance under realistic environmental conditions, and the best-performing solution was later implemented on a multi-floor commercial building in Riyadh, Saudi Arabia.

To streamline the analysis, simulations were conducted under 10 km/h wind speed with full sun exposure, as this condition reliably indicated performance outcomes. These additional simulation scenarios focused specifically on the 10 km/h windward condition during full sun exposure, as this was found to be a reliable indicator of a solution's performance based on the author's previous study [4]. This approach allowed for a meaningful comparison between the two wide mound options in terms of both thermal performance and design efficiency. In terms of surface area, both wide mound options had slightly higher values compared to the baseline façade, but the difference between them was relatively minor, as illustrated in Figure 21.

Buildings 2025, 15, 4130 24 of 32

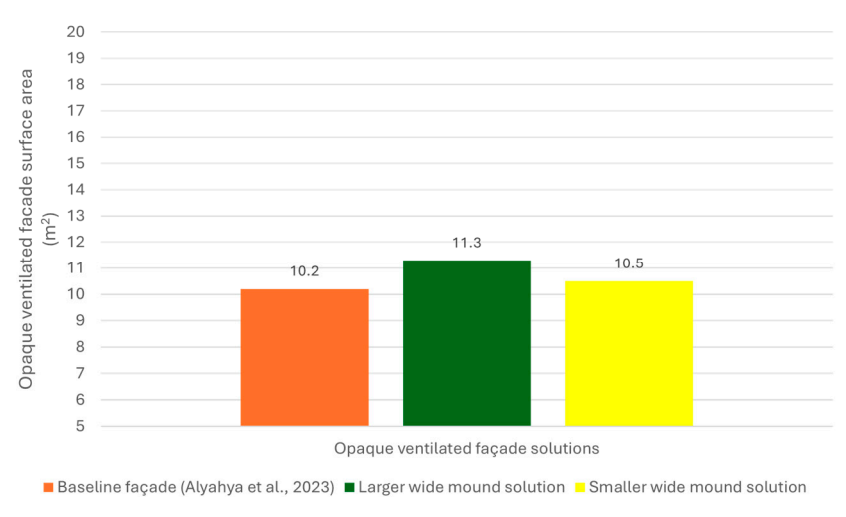


Figure 21. The total façade surface area of each solution in comparison to the baseline façade [3].

When assessing performance under different wind velocities, the larger wide mound solution consistently demonstrated better thermal performance than the smaller version. At all tested wind speeds (5, 10, and 20 km/h), the larger design exhibited lower average inner skin temperatures, with a maximum difference of 0.5 °C observed at lower wind speeds, as shown in Figure 22. Similarly, when wind direction varied, the larger wide mound performed slightly better, particularly under windward and side winds compared to the smaller option. Under leeward winds, both solutions had similar performance, as can be seen in Figure 22. In terms of solar exposure, both options behaved comparably under partial shading. However, the larger wide mound maintained a slight advantage when façades were fully exposed to the sun, as shown in Figure 22. Across all environmental scenarios, including variations in wind velocity, wind direction, and sun exposure, the larger wide mound solution consistently demonstrated better overall performance. While its thermal advantage over the smaller option was modest, it was consistent, and its surface area remained within a reasonable range. Overall, the larger wide mound solution proved to be the most effective in achieving the dual objectives of reducing both average inner skin surface temperature and façade surface area. Its consistent performance across varying environmental conditions made it the most suitable final choice for implementation.

3.2. Solution Application

The analysis has determined that the larger wide mound solution is the most optimal solution that can be achieved. Therefore, this solution has been implemented on a facade of three-floor commercial building in Riyadh, Saudi Arabia. This step verifies whether the performance of the optimal design remains comparable to that of the one that was measured and implemented on the $3\times3\times3$ m test cell, which represents a single-floor building. In addition, to demonstrate how the building appears from an architectural standpoint when represented in a manner that is nearly the same as the real building.

In order to match the earlier findings, the same CFD simulation settings were employed in this stage. An expanded domain was built around the building in order to capture all flow motions. This was necessary because the façade of the three-floor commercial building is larger than the single-floor test cell used in the entire study. The measurements of the tested three-floor larger wide mound solution in this section are 9 m in width and 9 m in height.

Since the previous optimal solutions comparison section reaffirmed that a 10 km/h windward during full sun exposure simulation is sufficient to provide an accurate indicator of a solution's performance, the CFD simulation results for this case were conducted under such conditions. The CFD simulation results yielded an interesting finding. The velocity

Buildings **2025**, 15, 4130 25 of 32

contour images of both the single-floor and the three-floor larger wide mound solutions are shown in Figure 23. Additionally, the average air velocity in the middle of the cavity is shown in this figure. It is evident that there was a noticeable increase in average air speed within the three-floor larger wide mound solution's cavity. The average air velocity in the cavity adjacent to only the lower floor of the three-floor larger wide mound solution, which is the first three meters from the ground, was 13.9 km/h, which is more than 43% faster than the velocity in the case of the single-floor larger wide mound solution. Consequently, the rise in the number of floors resulted in an advantageous influence on the average airflow velocity within the cavity.

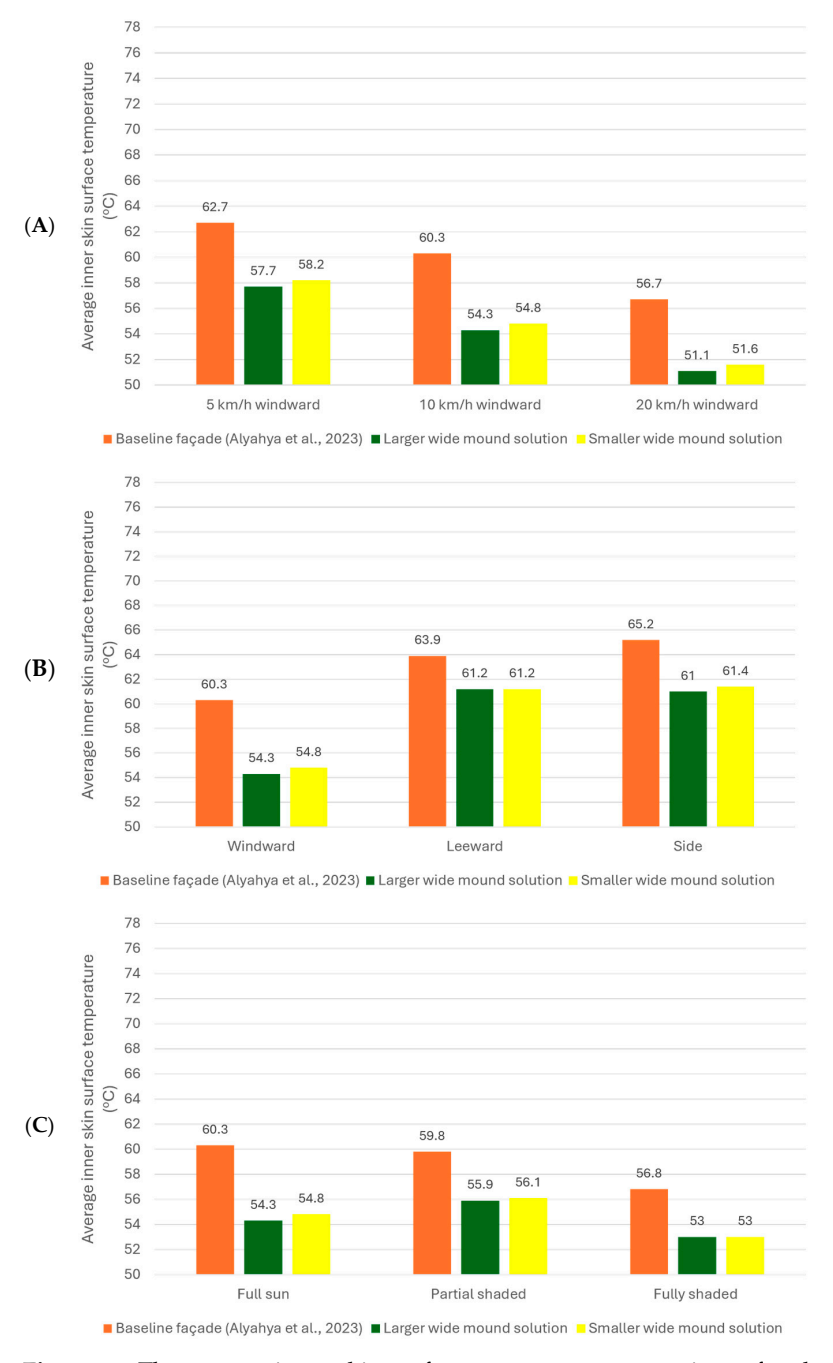


Figure 22. The average inner skin surface temperature comparison of each solution under varying environmental parameters: **(A)** wind velocity, **(B)** wind direction, and **(C)** solar exposure [3].

Buildings 2025, 15, 4130 26 of 32

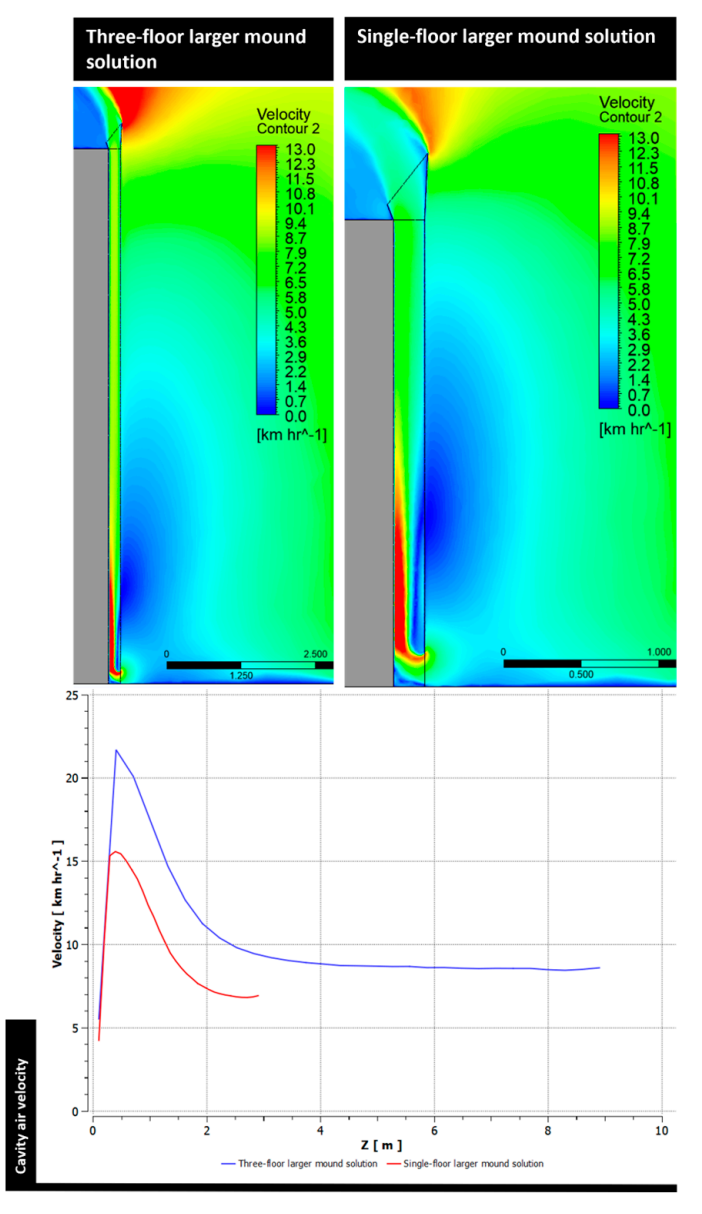


Figure 23. The velocity contour images and the average air velocity inside the cavity chart of both the single-floor and the three-floor larger wide mound solutions.

The rise in the average airflow velocity within the cavity of the three-floor larger wide mound solution led to a decrease in the average temperature of the inner skin surface, particularly on the lower floor, which experienced the highest average airflow speed. The average inner skin surface temperature on the lower floor was 53.0 $^{\circ}$ C, representing a reduction of 0.3 $^{\circ}$ C compared to the average inner skin surface temperature of the single-floor larger mound solution.

However, when the entire three-floor average inner surface temperature was taken into account, the average inner surface temperature of this three-floor larger wide mound solution was $55.6~^{\circ}$ C, as shown in Figure 24. In opaque ventilated facades, the stack or chimney effect occurs, which causes the warm air to rise, making it buoyant and pressing upward to exit the cavity through the outlet. This is the reason why the average temperature of the inner skin surface of the middle and upper floors increased. This was due to the fact that the air temperature inside the cavity had dramatically increased, as shown in Figure 25.

Buildings **2025**, 15, 4130 27 of 32

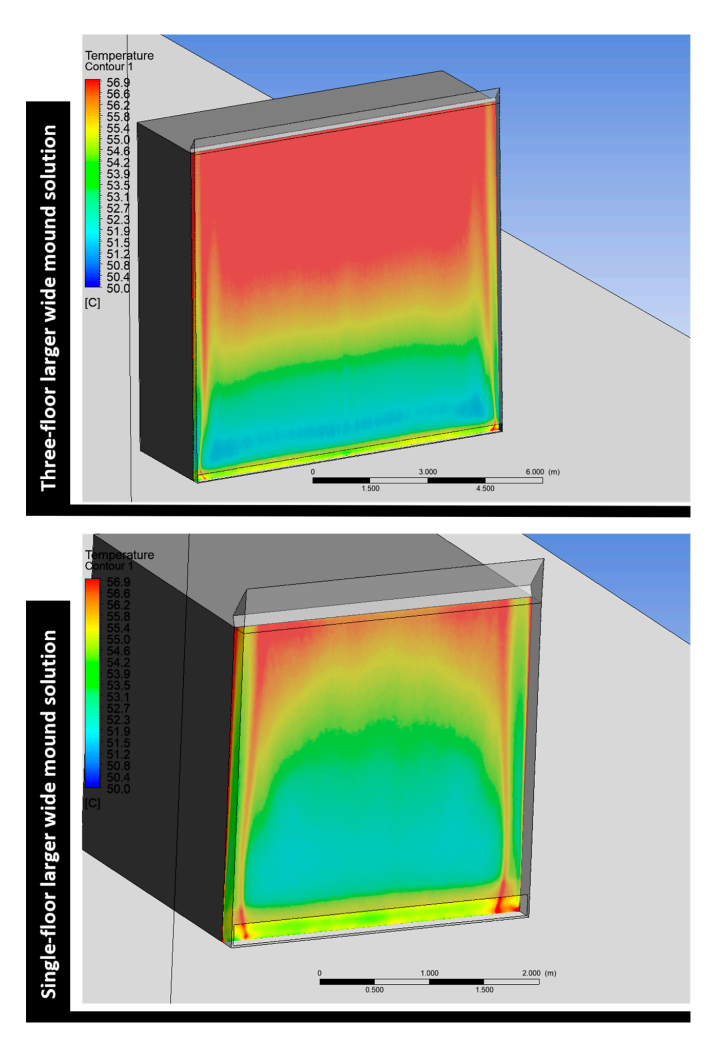


Figure 24. The average inner skin surface temperature of both the single-floor and the three-floor larger wide mound solutions.

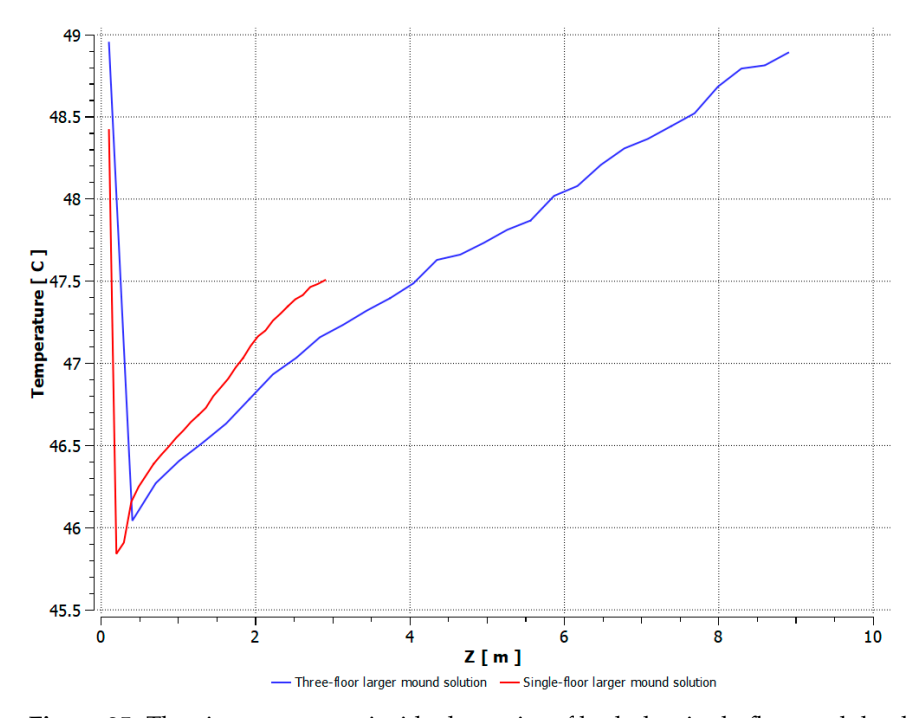


Figure 25. The air temperature inside the cavity of both the single-floor and the three-floor larger wide mound solutions.

Buildings 2025, 15, 4130 28 of 32

The application of the larger wide mound solution to low-rise buildings with multiple floors remains effective in enhancing the thermal performance of the opaque ventilated façade and substantially reducing the average inner skin surface temperature, without adversely affecting performance. However, there are situations in which the height of a floor can reach up to 5 m. This indicates that the solution for the three-floor larger wide mound should be examined not only when the total height is 9 m but also when it is 15 m. Another CFD simulation was carried out for a similar façade, but with a height of 15 m, to evaluate the effectiveness of this solution in lowering the average inner skin surface temperature. This 15 m-high façade can be viewed as either a tall three-floor building or a five-floor building, each 3 m tall.

The CFD simulation results clearly indicate a significant rise in average air speed within the cavity of the five-floor-wide mound solution, as depicted in Figure 26. The average air velocity in the cavity next to the lower floor was 15.6 km/h, over 60% faster than the velocity in the single-floor larger wide mound solution. As a result, the increased number of floors continued to have a positive effect on the average airflow velocity within the cavity.

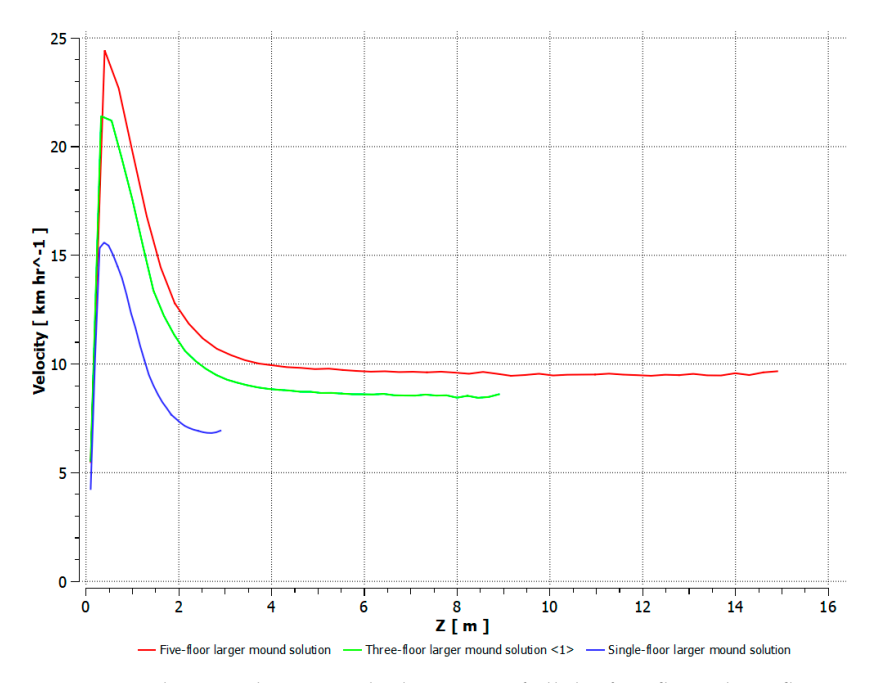


Figure 26. The air velocity inside the cavity of all the five-floor, three-floor and single-floor larger wide mound solutions.

The increased airflow velocity in the cavity of the five-floor larger wide mound solution resulted in a drop in the average temperature of the inner skin surface, especially on the lowest floor where the airflow speed was maximum, as shown in Figure 27. The average inner skin surface temperature on the lower floor was 52.5° C, which was 1.8° C lower than the average inner skin surface temperature of the single-floor larger wide mound solution. When the average inner surface temperature of the five floors was taken into consideration, the average inner skin surface temperature was 56.0° C. The difference between the average inner surface temperature of the three-floor larger wide mound solution and the average inner surface temperature of the five-floor solution was only 0.4° C higher. This indicates that even when the facade reaches 15 m, this solution continues to be effective in improving the thermal performance of the opaque ventilated façade.

Buildings 2025, 15, 4130 29 of 32

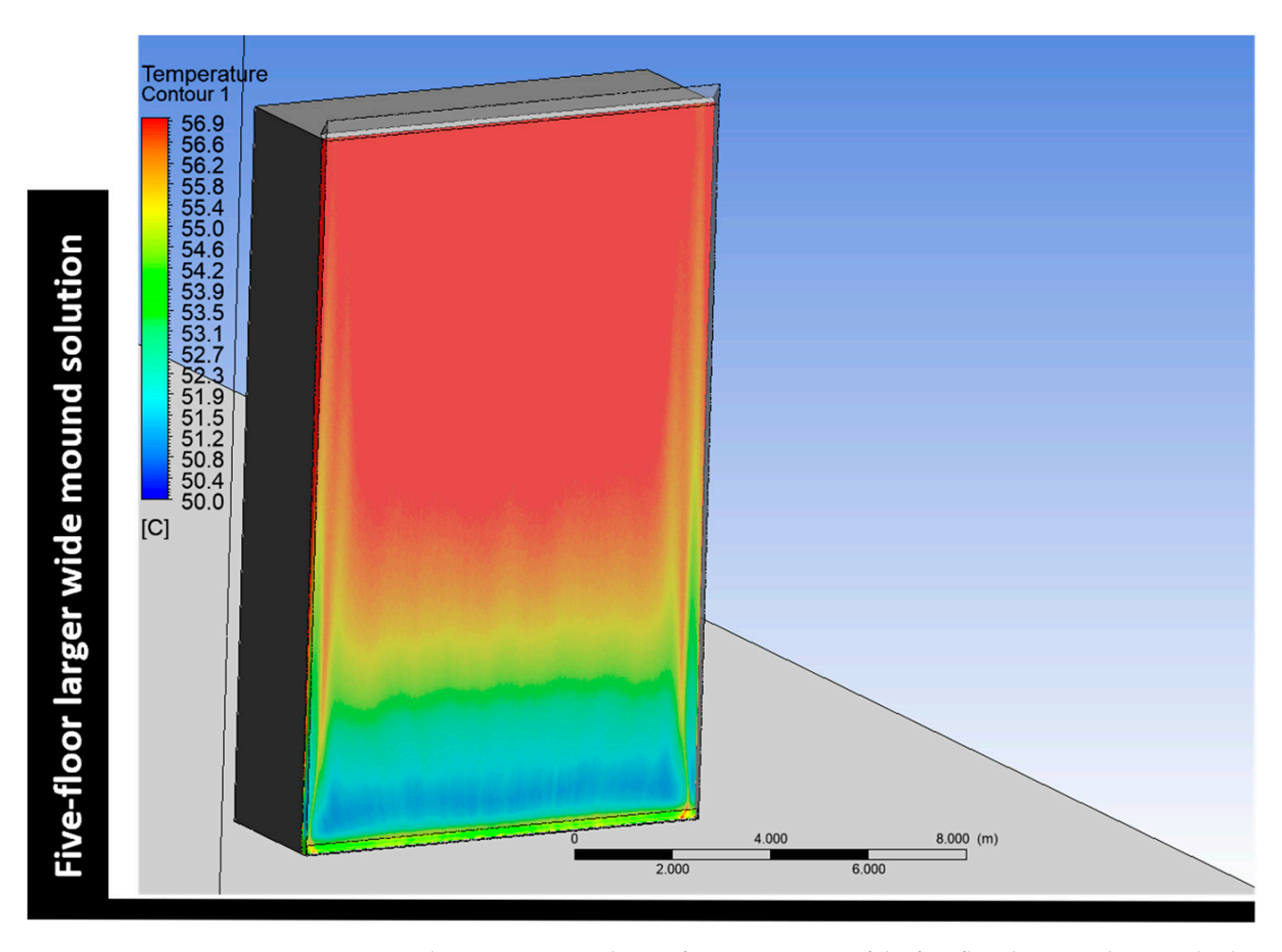


Figure 27. The average inner skin surface temperature of the five-floor larger wide mound solutions.

When applied to a three-story commercial building in Riyadh, Saudi Arabia, the larger wide mound façade solution demonstrates its potential for seamless architectural integration. One of the most notable advantages of this system is its versatility, allowing it to be incorporated into a wide range of building designs without requiring alterations to the original façade concept. As shown in Figure 28, the façade retains a conventional appearance when viewed from the human perspective. The only visible distinction is a 20 cm elevation from the ground, which serves as the air inlet to the concealed cavity. This minimal change allows architects to implement the solution without compromising their intended design vision. Furthermore, the system supports a variety of outer skin materials, enabling it to adapt to different architectural styles and esthetics, as can be seen in Figure 28. This flexibility ensures that the façade can be customized to meet the specific visual goals of each project. In terms of constructability, the proposed design follows standard practices for opaque ventilated façades. The additional top wide mound component can be fabricated using conventional or digital manufacturing methods and installed on top of the façade without the need for specialized labor, making the system both practical and efficient to implement.

Buildings **2025**, 15, 4130 30 of 32



Figure 28. The appearance of the larger wide mound solution on a three-floor commercial building in Riyadh, Saudi Arabia.

4. Conclusions

This study presented an integrated computational framework for the multi-objective optimization of biomimetic opaque ventilated façades (OVFs) tailored to hot arid climates. By combining parametric modeling, CFD simulations, and machine learning-based surrogate models within the Ansys DesignXplorer environment, the research demonstrated an

Buildings 2025, 15, 4130 31 of 32

efficient and scalable approach for optimizing complex façade systems. A key contribution of this research is the novel application of machine learning algorithms to accurately predict CFD simulation outcomes for opaque ventilated façades. This predictive capability allowed for the generation and evaluation of a vast number of design alternatives without the need for time-intensive real-time simulations. Additionally, the study established a direct link between parametric modeling tools and CFD simulations, enabling the development of a fully computationally optimized façade design grounded in performance-based criteria.

This framework offers several advantages, including reduced computational time, the ability to evaluate a large number of design configurations, and strong predictive capability. However, some limitations remain, particularly the restricted access to internal machine learning parameters and reliance on automated algorithms within the software environment. Recognizing these aspects helps guide future improvements in the transparency and adaptability of similar optimization workflows.

The optimization process identified the larger wide mound configuration as the most effective solution, demonstrating superior thermal performance compared to the original bio-inspired geometry. Subsequent simulation scenarios and building-scale applications confirmed the practical viability of this biomimetic OVF design. When implemented in low-rise commercial buildings in hot desert regions, the design significantly reduced the inner skin surface temperature and enhanced overall thermal performance. Moreover, it proved to be constructible using conventional façade techniques and adaptable to various architectural styles without requiring alterations to the external appearance.

Future research should focus on refining airflow control strategies, such as adjusting vent sizes and introducing intermediate or adjustable vents. Further investigation into long-term energy performance, real-world prototyping, and integration with smart building systems will also help advance the applicability of biomimetic OVFs in diverse climatic contexts.

Overall, this research advances the field by introducing a replicable, performance-driven workflow that integrates bio-inspired design, simulation-based optimization, and machine learning. The findings support the development of high-performance building envelopes in extreme climate conditions and open avenues for further exploration into lifecycle performance, real-world prototyping, and broader architectural integration.

Author Contributions: Conceptualization, A.A.; Data curation, A.A.; Formal analysis, A.A.; Investigation, A.A., S.L. and W.J.; Methodology, A.A.; Resources, A.A.; Software, A.A.; Supervision, S.L. and W.J.; Validation, A.A. and S.L.; Visualization, A.A.; Writing—original draft, A.A.; Writing—review and editing, A.A. All authors have read and agreed to the published version of the manuscript.

Funding: This research received no external funding.

Data Availability Statement: The original contributions presented in this study are included in the article. Further inquiries can be directed to the corresponding author.

Acknowledgments: This work is based on Ahmed Alyahya's doctoral dissertation. Some sections of the text closely follow or replicate the original content from my PhD thesis and have been included here with the consent of the editors.

Conflicts of Interest: The authors declare no conflicts of interest.

References

- Ibañez-Puy, M.; Vidaurre-Arbizu, M.; Sacristán-Fernández, J.A.; Martín-Gómez, C. Opaque Ventilated Façades: Thermal and energy performance review. Renew. Sustain. Energy Rev. 2017, 79, 180–191. [CrossRef]
- 2. Sotelo-Salas, C.; del Pozo, C.E.; Esparza-López, C.J. Thermal assessment of spray evaporative cooling in opaque double skin facade for cooling load reduction in hot arid climate. *J. Build. Eng.* **2021**, *38*, 102156. [CrossRef]

Buildings 2025, 15, 4130 32 of 32

3. Alyahya, A.; Lannon, S.; Jabi, W. CFD simulation for opaque ventilated facades in hot arid climate based on literature review design parameters. In Proceedings of the Building Simulation 2023: 18th Conference of IBPSA, Shanghai, China, 4–6 September 2023; Volume 18, pp. 909–916. [CrossRef]

- 4. Alyahya, A.; Lannon, S.; Jabi, W. Biomimetic Opaque Ventilated Façade for Low-Rise Buildings in Hot Arid Climate. *Buildings* **2025**, *15*, 2491. [CrossRef]
- 5. Jabi, W. Parametric Design for Architecture; Laurence King Publishing: London, UK, 2013.
- 6. McNeel. Grasshopper. [Online]. Available online: https://www.grasshopper3d.com/ (accessed on 26 May 2023).
- 7. ANSYS. ANSYS Fluent User's Guide; ANSYS: Canonsburg, PA, USA, 2022.
- 8. ANSYS. ANSYS DesignXplorer User 's Guide; ANSYS: Canonsburg, PA, USA, 2023.
- 9. Palkovič, A.; Pečený, P.; Teichman, J. Optimization of pressure drop in curved conduits using Ansys DesignXplorer. *MATEC Web Conf.* **2022**, *367*, 00019. [CrossRef]
- 10. Ayancik, F.; Acar, E.; Celebioglu, K.; Aradag, S. Simulation-based design and optimization of Francis turbine runners by using multiple types of metamodels. *Proc. Inst. Mech. Eng. Part C J. Mech. Eng. Sci.* **2016**, 231, 1427–1444. [CrossRef]
- 11. Kaseb, Z.; Montazeri, H. Data-driven optimization of building-integrated ducted openings for wind energy harvesting: Sensitivity analysis of metamodels. *Energy* **2022**, *258*, 124814. [CrossRef]
- 12. Fallahpour, M.; Khorshidi, I.M.; Ghasempour, F.; Davari, D.D.; Khoei, E.T.; Tamimi, M. A multi-objective optimization framework for designing a double-skin façade in hot-arid climate: Central composite design and CFD simulation. *Results Eng.* **2025**, 25, 104288. [CrossRef]
- 13. Abdeen, A.; Serageldin, A.A.; Ibrahim, M.G.E.; El-Zafarany, A.; Ookawara, S.; Murata, R. Solar chimney optimization for enhancing thermal comfort in Egypt: An experimental and numerical study. *Sol. Energy* **2019**, *180*, 524–536. [CrossRef]
- 14. Szpisják-Gulyás, N.; Al-Tayawi, A.N.; Horváth, Z.H.; László, Z.; Kertész, S.; Hodúr, C. Methods for experimental design, central composite design and the Box–Behnken design, to optimise operational parameters: A review. *Acta Aliment.* **2023**, *52*, 521–537. [CrossRef]

Disclaimer/Publisher's Note: The statements, opinions and data contained in all publications are solely those of the individual author(s) and contributor(s) and not of MDPI and/or the editor(s). MDPI and/or the editor(s) disclaim responsibility for any injury to people or property resulting from any ideas, methods, instructions or products referred to in the content.